Intermediate filament-associated cytolinker plectin 1c destabilizes microtubules in keratinocytes

Rocio G. Valencia[a], Gernot Walko[a], Lubomir Janda[a,b], Jirka Novacek[b], Eva Mihailovska[a], Siegfried Reipert[a], Kerstin Andrä-Marobela[a,*], and Gerhard Wiche[a]

[a]Max F. Perutz Laboratories, Department of Biochemistry and Cell Biology, University of Vienna, A-1030 Vienna, Austria; [b]Center for Structural Biology, Division of Biomolecular NMR Spectroscopy, Central European Institute of Technology, Masaryk University, CZ-62500 Brno, Czech Republic

ABSTRACT **The transition of microtubules (MTs) from an assembled to a disassembled state plays an essential role in several cellular functions. While MT dynamics are often linked to those of actin filaments, little is known about whether intermediate filaments (IFs) have an influence on MT dynamics. We show here that plectin 1c (P1c), one of the multiple isoforms of the IF-associated cytolinker protein plectin, acts as an MT destabilizer. We found that MTs in P1c-deficient (P1c$^{-/-}$) keratinocytes are more resistant toward nocodazole-induced disassembly and display increased acetylation. In addition, live imaging of MTs in P1c$^{-/-}$, as well as in plectin-null, cells revealed decreased MT dynamics. Increased MT stability due to P1c deficiency led to changes in cell shape, increased velocity but loss of directionality of migration, smaller-sized focal adhesions, higher glucose uptake, and mitotic spindle aberrations combined with reduced growth rates of cells. On the basis of ex vivo and in vitro experimental approaches, we suggest a mechanism for MT destabilization in which isoform-specific binding of P1c to MTs antagonizes the MT-stabilizing and assembly-promoting function of MT-associated proteins through an inhibitory function exerted by plectin's SH3 domain. Our results open new perspectives on cytolinker-coordinated IF-MT interaction and its physiological significance.**

Monitoring Editor
Robert D. Goldman
Northwestern University

Received: Jun 29, 2012
Revised: Nov 14, 2012
Accepted: Jan 18, 2013

This article was published online ahead of print in MBoC in Press (http://www.molbiolcell.org/cgi/doi/10.1091/mbc.E12-06-0488) on January 30, 2013.

*Present address: Department of Biological Sciences (CESRIKI), University of Botswana, Gaborone, Botswana.

Address correspondence to: Gerhard Wiche (gerhard.wiche@univie.ac.at).

Abbreviations used: 2-NBDG, 2-[N-(7-nitrobenz-2-oxa-1,3-diazol-4-yl)amino]-2-deoxy-D-glucose; ABD, actin-binding domain; CI, confidence interval; CMPI, Complete Mini Protease Inhibitor Cocktail tablets; DMSO, dimethyl sulfoxide; DTT, dithiothreitol; EGFP, enhanced green fluorescent protein; EGTA, ethylene glycol tetraacetic acid; EM, electron microscopy; FA, focal adhesion; GFP, green fluorescent protein; GST, glutathione *S*-transferase; HMW, high molecular weight; HRP, horseradish peroxidase; HS-SN, high-speed supernatant; IB, immunoblotting; IF, intermediate filament; IFM, immunofluorescence microscopy; IgG, immunoglobulin G; IP, immunoprecipitation; MAP, microtubule-associated protein; MT, microtubule; NA, numerical aperture; P0, plectin-null; P1a, plectin 1a; P1c, plectin 1c; PBS, phosphate-buffered saline; PC, phosphocellulose; PMSF, phenylmethylsulfonyl fluoride.

INTRODUCTION

Cytolinker proteins play a key role in strengthening cells against mechanical stress and in regulating cytomatrix plasticity by networking and anchoring cytoskeletal filament systems to organelles and junctional complexes. Plectin, a protein of very large size (>500 kDa), is a member of the cytolinker protein family and one of the most abundant and versatile cytolinkers expressed in mammalian cells (for reviews, see Wiche, 1998; Wiche and Winter, 2011). One of plectin's outstanding features is its functional diversity, which is mainly based on alternative splicing of a series of different first coding exons (Fuchs *et al.*, 1999). A variety of isoforms generated in this way differ only in short N-terminal sequences that specify distinct properties of the cytolinker, including its cellular targeting and N-terminal binding partners (Rezniczek *et al.*, 2003, 2004; Abrahamsberg *et al.*, 2005; Winter *et al.*, 2008; Burgstaller *et al.*, 2010). Common to all isoforms is their single-exon-encoded ~200-kDa C-terminal domain, which contains plectin's intermediate filament (IF) binding site(s) (Nikolic *et al.*, 1996). In interacting

with all types of IFs via their C-termini and associating with distinct targets via their N-termini, plectin isoforms turned out to be essential for IF cytoarchitecture and therefore for general cell integrity, as recently demonstrated for skeletal muscle using conditional and isoform-specific knockout mice (Konieczny *et al.*, 2008; Wiche and Winter, 2011). Moreover, as a scaffolding platform and regulator of IF network architecture, plectin and some of its isoforms have been shown to affect signaling pathways and basic cell functions, including cell migration, polarization, stress response, and mitochondrial fusion/fission events (Osmanagic-Myers and Wiche, 2004; Osmanagic-Myers *et al.*, 2006; Abrahamsberg *et al.*, 2005; Gregor *et al.*, 2006; Winter *et al.*, 2008; Burgstaller *et al.*, 2010).

In basal keratinocytes, in which keratin IFs are linked to hemidesmosomal integrin β4 via plectin isoform 1a (P1a; Andrä *et al.*, 2003; Kostan *et al.*, 2009), plectin deficiency leads to the skin-blistering disease epidermolysis bullosa simplex (Gache *et al.*, 1996; Smith *et al.*, 1996; for a recent review, see Winter and Wiche, 2013), as mimicked by plectin-null (P0) and conditional plectin knockout mice (Andrä *et al.*, 1997; Ackerl *et al.*, 2007). The role of plectin 1c (P1c), a second isoform of plectin expressed in epithelial cells at high levels (Andrä *et al.*, 2003; Walko *et al.*, 2011), is unknown. Not unexpectedly, P1c is also a major isoform of neural cells (Fuchs *et al.*, 1999) that share with epidermal cells a common developmental origin, the ectoderm. P1c deficiency in mice leads to reduced nerve conduction velocity in motor neurons (Fuchs *et al.*, 2009).

We have shown previously that plectin and, by implication, plectin-modulated IF network cytoarchitecture regulate actin dynamics (Andrä *et al.*, 1998). In the present study, we tested whether a similar concept applies to microtubules (MTs) by studying the role of P1c as a regulator of MT dynamics in keratinocytes. A number of observations made in previous studies, including the in vitro binding of neural plectin to microtubule-associated proteins (MAPs; Herrmann and Wiche, 1987), the visualization of plectin sidearms mediating IF-MT interaction (Svitkina *et al.*, 1996), the targeting of overexpressed P1c to MTs (Rezniczek *et al.*, 2003), and the partial colocalization of P1c with MTs in cultured cells (Andrä *et al.*, 2003), pointed toward a likely interaction of plectin with MTs. Moreover, ACF7 and BPAG1, other members of the plakin cytolinker protein family, have been shown to be involved in the regulation of MT dynamics, with both acting as MT stabilizers (Yang *et al.*, 1999; Kodama *et al.*, 2003; Wu *et al.*, 2008).

We report here that, contrary to other previously studied cytolinker proteins, P1c acts as a destabilizer of MTs. Functioning as a promoter of MT dynamics, plectin was found by us to affect vital MT-dependent functions and properties of keratinocytes, including focal adhesion (FA) turnover, shape and polarized migration of cells, glucose uptake, cell division, and growth. On the basis of a combination of data from ex vivo approaches and in vitro experiments using purified proteins, we also provide a model for a possible molecular mechanism of MT destabilization through IF-bound plectin.

RESULTS

Altered MT network organization in plectin-deficient keratinocytes: is P1c a MAP?

MTs are dynamic polymers that change their organization and distribution during the cell cycle and upon differentiation of cells, such as during polarization of epithelia (Lechler and Fuchs, 2007; Bowen *et al.*, 2011). To study the effects of plectin deficiency on MT organization in stratifying keratinocytes, we exposed immortalized mouse wild-type and P0 keratinocytes to elevated levels of Ca^{2+} to induce the formation of cell–cell junctions and initiate stratification. Immunostaining of either cell type grown at 0.05 mM (low) Ca^{2+}, using anti–α-tubulin antibodies, revealed typical MT networks radiating from the nucleus toward the cell periphery, without noticeable differences of staining patterns (Figure 1A, top panels, Wt and P0). However, upon stratification in 1.8 mM (high) Ca^{2+}, P0 keratinocytes displayed MT bundles that appeared more densely packed than those of wild-type cells (Figure 1A, bottom panels, Wt and P0). This phenotype could be confirmed on the ultrastructural level by examining embedded thin sections of stratifying wild-type and P0 keratinocyte monolayers by electron microscopy (EM; Supplemental Figure S1).

These observations supported the idea that plectin may play a role in MT network organization with possible implications for MT functions. Having identified a unique role of P1a in hemidesmosome homeostasis (Walko *et al.*, 2011), we wondered whether the other major isoform of plectin expressed in keratinocytes, P1c, could be involved in MT network organization. In fact, when immortalized wild-type keratinocytes were subjected to double immunofluorescence microscopy (IFM) using anti-tubulin and isoform P1c-specific antibodies, cytoplasmic P1c was found to partially colocalize with MTs, mostly in a dotted pattern (Figure 1B). This staining pattern was clearly distinguishable from that of hemidesmosome-associated P1a (see Andrä *et al.*, 2003; Kostan *et al.*, 2009). Furthermore, when primary P1c-deficient ($P1c^{-/-}$) keratinocytes derived from isoform-specific knockout mice (Fuchs *et al.*, 2009) were exposed to 1.8 mM Ca^{2+}, they displayed densely packed MT bundles after stratification (Figure 1A, $P1c^{-/-}$ panels).

To assess whether P1c bound directly to MTs, we carried out cosedimentation assays using preassembled (Taxol-stabilized) brain MTs as an affinity matrix for MT-binding proteins present in soluble cell extracts of wild-type keratinocytes. Although the two major keratinocyte isoforms P1a and P1c were present in such extracts in comparable amounts, P1c, contrary to P1a, showed partial cosedimentation with MTs (Figure S2), consistent with the possibility of plectin-MT binding being isoform-specific.

MTs in P1c-deficient keratinocytes are more resistant to MT-depolymerizing drugs and show increased acetylation

Proteins that bind along MTs often are responsible for altering the mechanical properties of the polymer, either by its stabilization (e.g., MAPs, ACF7/MACF) or destabilization (e.g., Op18/stathmin, SCG10; for a review, see Conde and Cáceres, 2009). To investigate whether P1c shares such properties and to analyze its specific role in MT network organization, we first examined whether the absence of P1c affected the sensitivity of MTs to the MT-depolymerizing drug nocodazole (Figure 2A). By tracing and quantifying MTs that remained polymerized after treatment of primary keratinocytes with low doses of the drug, we unexpectedly found MTs in $P1c^{-/-}$ keratinocytes to be more resistant to depolymerization compared with those in wild-type cells (Figure 2A, $P1c^{-/-}$ and Wt). A similar phenomenon was observed when MTs in P0 keratinocytes were analyzed (Figure 2A, P0). These data suggested that MTs were more stable in plectin-deficient compared with wild-type keratinocytes.

As stable populations of MTs usually are enriched in posttranslationally acetylated α-tubulin (Piperno *et al.*, 1987; Bulinski *et al.*, 1988), we investigated the distribution and quantified the levels of acetylated tubulin in primary $P1c^{-/-}$, wild-type, and P0 keratinocytes. Subjecting cells to IFM, using anti-tubulin antibodies in combination with antibodies specific for acetylated tubulin, we found that only the central part of the cells was stained for acetylated tubulin in wild-type keratinocytes, whereas acetylated MTs were extending from the center of the cell up to its periphery in both mutant cell types ($P1c^{-/-}$ and P0; Figure 2B). The quantification

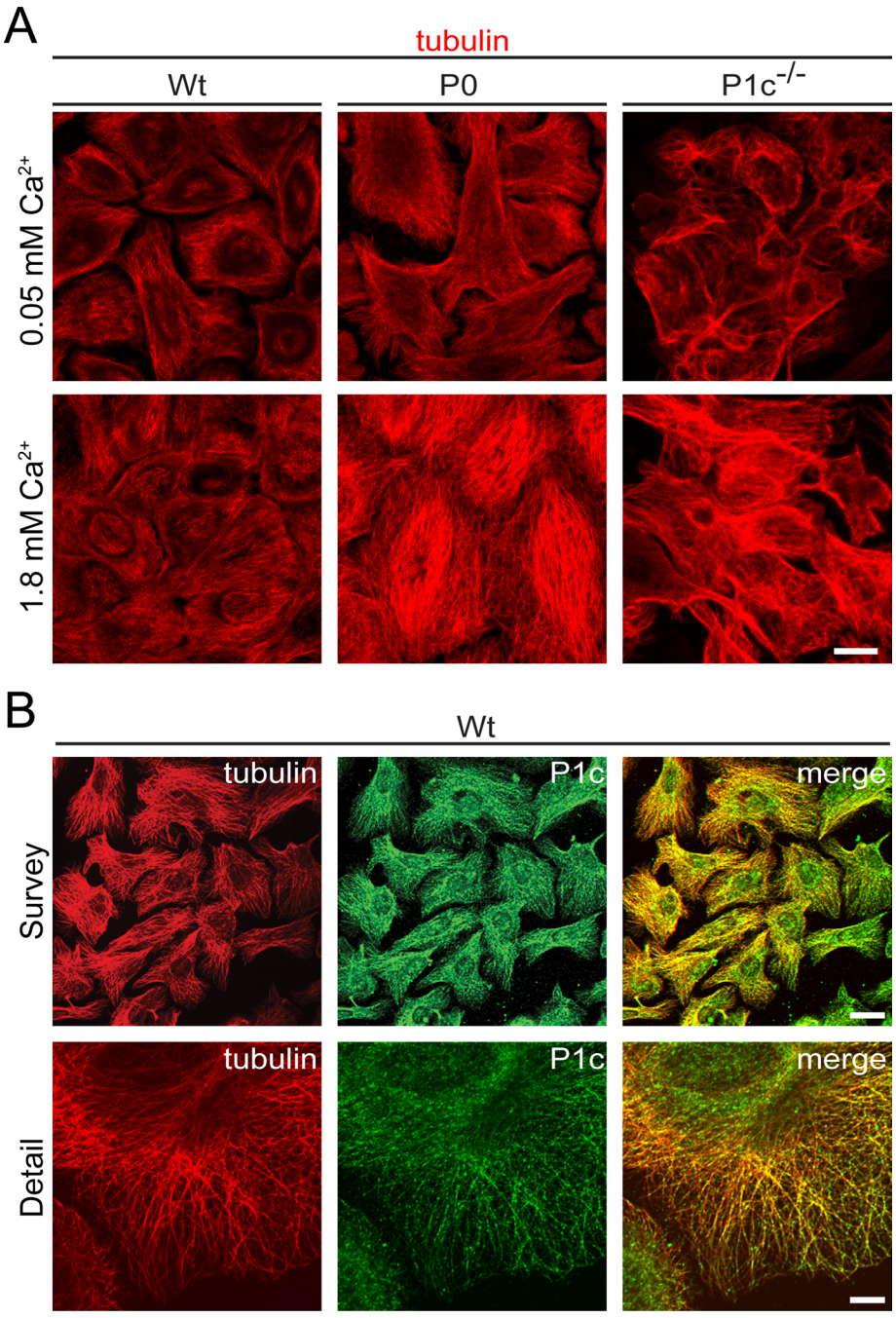

FIGURE 1: P1c interacts with MTs and affects MT cytoarchitecture. (A) IFM of undifferentiated (0.05 mM Ca^{2+}) and stratifying (1.8 mM Ca^{2+}) immortalized wild-type (left column), immortalized P0 keratinocytes (middle column), and primary $P1c^{-/-}$ (right column) keratinocytes, using antibodies to tubulin. Note higher density of MT bundles, particularly in peripheral regions, in differentiated P0 and $P1c^{-/-}$ compared with wild-type cells. Scale bar: 20 μm. (B) Double IFM of immortalized wild-type keratinocytes using anti–α-tubulin and anti–isoform P1c–specific antibodies. Note immunolocalization of P1c all over the cytoplasm (survey) and P1c dotted decoration of MTs (detail). Scale bars: 50 μm (top row); 10 μm (bottom row).

(in pixels) of acetylated tubulin-positive areas versus unmodified (total) tubulin-positive areas (for further details, see *Materials and Methods*) showed the acetylated form to be approximately threefold increased in plectin-deficient ($P1c^{-/-}$ and P0) keratinocytes compared with wild-type cells (Figure 2B). Increased acetylation of tubulin in plectin-deficient keratinocytes was confirmed by immunoblotting (IB) analysis of cell extracts prepared from proliferating (0.05 mM Ca^{2+}), as well as stratifying (1.8 mM Ca^{2+}), keratinocytes (Figure 2C).

Reversal of MT stabilization in $P1c^{-/-}$ keratinocytes requires full-length P1c

To assess whether MT stabilization in mutant cells was directly linked to P1c deficiency, we performed rescue experiments in which primary $P1c^{-/-}$ keratinocytes were transiently transfected with cDNA expression plasmids encoding enhanced green fluorescent protein (EGFP) fusion proteins with either full-length P1c (P1c-EGFP) or one of two N-terminal fragments of P1c: a shorter one (P1c-8-EGFP) comprising the N-terminal actin-binding domain (ABD) preceded by the isoform-specific, exon 1c–encoded sequence; and a similar longer one (P1c-30-EGFP) extending to plectin's central α-helical coiled-coil rod domain (see also Figure 8A later in the paper). On forced expression, P1c-EGFP was found accumulated at filamentous structures around the nucleus but was visualized also in a dotted pattern throughout the cytoplasm (Figure 3A, top panels). In contrast, P1c-8-EGFP colocalized with stress fibers (Figure 3A, middle panels), as has previously been described (Rezniczek *et al.*, 2003). P1c-30-EGFP was found associated with filamentous structures throughout the cytoplasm (Figure 3A, bottom panels). When MTs in transfected cells were exposed to nocodazole to assess their resistance toward drug-induced disassembly, we found that full-length P1c expression led not only to a reversal of the phenotype but even to an overshooting effect (Figure 3A, bar graph), that is, destabilization of MTs to levels below that of wild-type cells, probably due to overexpression of P1c to levels higher than normal. In contrast with full-length P1c, expression of the truncated versions P1c-8 and P1c-30 did not effect a statistically significant reduction of MT stability, as revealed by the abundant presence of MTs remaining after nocodazole treatment (Figure 3A, middle and bottom panels). In control experiments using primary $P1c^{-/-}$ keratinocytes without nocodazole challenge, no MT-depolymerizing effects of any of the cDNA constructs used for transfection were detectable (Figure S3). When MT acetylation was measured upon transfection of cells in a similar series of experiments, again only full-length P1c led to a partial restoration of the phenotype (Figure 3B), that is, a reduction of acetylated MT signals.

Together, these data strongly suggested that P1c indeed was destabilizing rather than stabilizing MTs, contrary to what had been observed with other cytolinker protein family members, such as ACF7/MACF and BPAG1 (Yang *et al.*, 1999; Kodama *et al.*, 2003). Moreover, the results obtained using truncated forms of P1c suggested that the full-length protein containing the IF-binding site

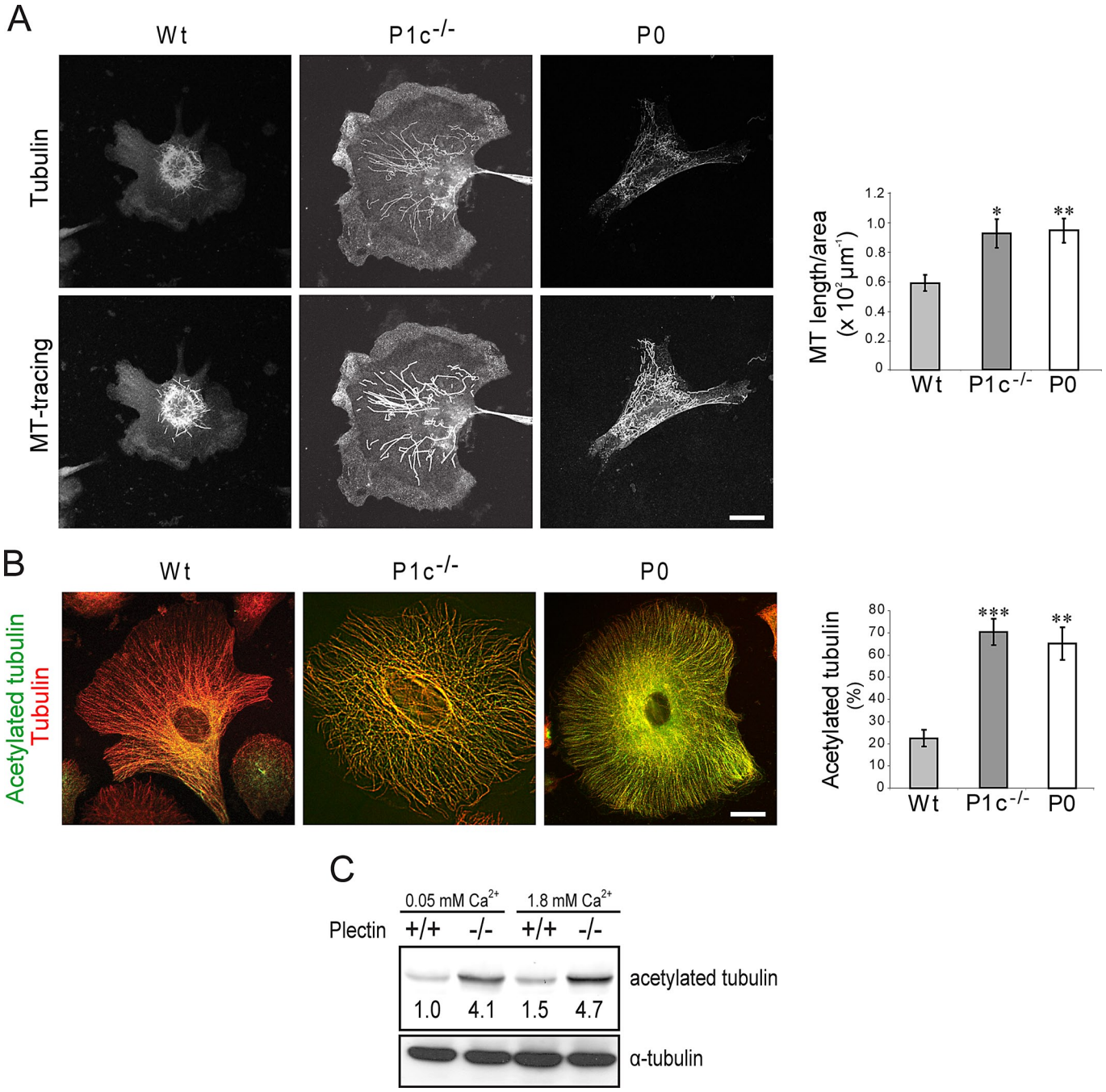

FIGURE 2: P1c affects the stability of keratinocyte MTs. (A) Nocodazole-treated primary wild-type, P1c$^{-/-}$, and P0 keratinocytes were immunolabeled using antibodies to α-tubulin (tubulin), and drug-resistant MTs remaining in cells were traced (MT-tracing) and quantified ($n = 5$; 20 cells/experiment). (B) The proportions of acetylated (green) MTs present in primary keratinocytes of the types indicated, were analyzed using rat mAbs to tubulin and mouse mAbs to acetylated tubulin. Statistical evaluations as in (A). (A and B) Scale bars: 20 µm. Error bars: ± 95% confidence interval (CI). *, $p < 0.05$; **, $p < 0.01$; ***, $p < 0.001$. (C) Quantification (IB) of acetylated tubulin present in cell lysates from immortalized wild-type and P0 keratinocytes prior to (0.05 mM Ca^{2+}) and after exposure (3 h) to 1.8 mM Ca^{2+}. Numbers are quantified relative levels of acetylated tubulin.

was required in order to reset MT stability to the less-stable state of wild-type cells.

P1c deficiency affects MT dynamics

To explore whether the increased stability of MTs observed in plectin-deficient cells was reflected in their dynamic behavior, we first transfected keratinocytes with EGFP-tagged tubulin (Krylyshkina *et al.*, 2002), enabling the visualization of rapidly shortening (catastrophe) and regrowing (rescue) MTs at the cell margins. These experiments were restricted to immortalized wild-type and P0 keratinocyte cell lines, as the quality of transfection achieved with this expression plasmid in primary keratinocytes was insufficient for time-lapse studies. In addition to measuring catastrophe and rescue frequencies of MTs, we quantified the proportions of MTs that were

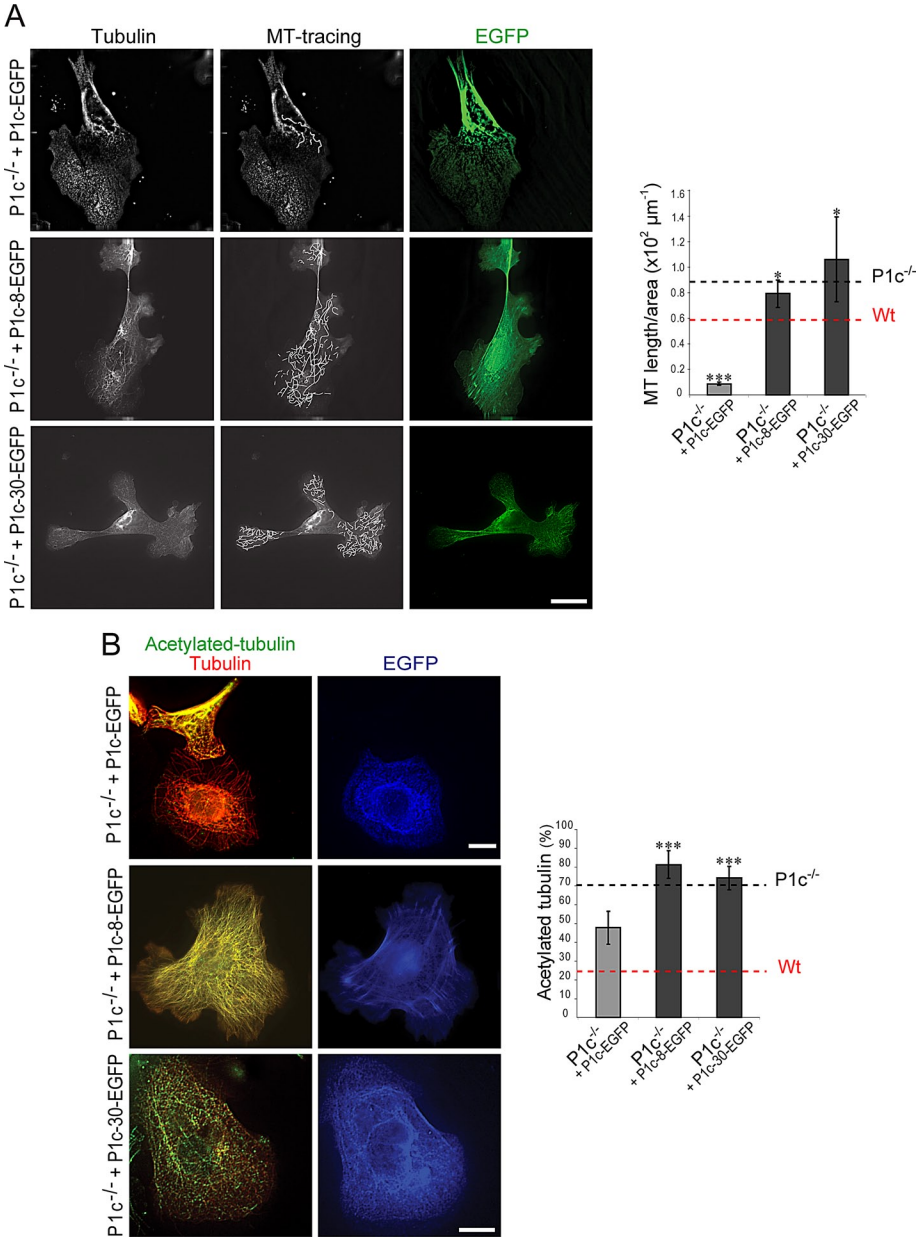

FIGURE 3: P1c variants lacking the IF-binding domain fail to reverse MT stabilization in P1c-deficient keratinocytes. (A) Nocodazole-treated primary P1c$^{-/-}$ keratinocytes transfected with full-length P1c-EGFP (top row), P1c8-EGFP (middle row), and P1c-30-EGFP (bottom row) were immunolabeled using antibodies to α-tubulin (tubulin) and drug-resistant MTs remaining in cells were traced (MT tracing). Bar graph shows quantification of the MT length normalized to total cell area; red and black broken lines indicate corresponding values measured for wild-type and P1c$^{-/-}$ cells, respectively (see Figure 2A) ($n = 3$; 6 cells/experiment). Error bars: ± 95% CI. *, $p < 0.05$; ***, $p < 0.001$. Scale bar: 15 µm. (B) The proportion of acetylated tubulin present in primary P1c$^{-/-}$ keratinocytes expressing full-length or truncated versions of P1c (see A) was determined by IFM, as described in Figure 2B. Channels: red, tubulin; green, acetylated tubulin; blue, EGFP. Scale bars: 15 µm (top row); 10 µm (middle and bottom rows). Bar graph represents statistical evaluations as in (A).

growing perpendicularly toward the membrane versus those bending or sliding along the membrane. The results revealed a nearly identical rescue frequency in wild-type and P0 cells, but an ~2.5-fold decrease of catastrophe frequency in P0 compared with wild-type cells (Figure 4, A and B); this was consistent with the higher stability of MTs observed in mutant cells (see Figure 2A). Interestingly, in wild-type cells, most of the MTs were growing perpendicularly toward the membrane and upon reaching it underwent rapid disassembly (catastrophe; Figure 4A and Supplemental Video S1), while P0 cells showed a higher percentage of MTs that, upon reaching the membrane, were bending or sliding along it, rather than disassembling (Figure 4C and Video S1).

To investigate the growth parameters of MTs in more detail and to include primary P1c$^{-/-}$ keratinocytes in the analysis, we performed time-lapse microscopy of MTs labeled with green fluorescent protein (GFP)-tagged EB1 (Stepanova *et al.*, 2003), a +TIP protein family member that binds to the growing (plus) ends of MTs (Su *et al.*, 1995; Akhmanova and Steinmetz, 2008). Interestingly, time-lapse images of GFP-EB1–transfected P1c$^{-/-}$ keratinocytes revealed that MTs in P1c$^{-/-}$ keratinocytes were more static than those in wild-type and P0 cells (for survey views, see Videos S2–S4). Measuring the time that growing MTs spent pausing (without disassembly), we found that P1c$^{-/-}$ MTs were pausing on average ~4.6 times longer than wild-type MTs (Figure 4D), whereas P0 MTs spent less time for pausing than did their wild-type counterparts. This difference in the behavior of P1c$^{-/-}$ and P0 MTs regarding pausing may indicate an isoform P1c$^{-/-}$-specific phenotype that probably was obscured in P0 cells due to the absence of other plectin isoforms. When the growth rates of EB1 comets between pauses were measured, MT tips were found to grow faster in both mutant cell types (P0 and P1c$^{-/-}$) compared with wild-type cells (Figure 4E and Video S5). Most importantly, MTs in both P0 and P1c$^{-/-}$ mutant cell types failed to undergo catastrophe after reaching the cell margins but continued to grow, undergoing bending at the periphery, contrary to wild-type MTs, which paused upon reaching the cell membrane before disappearing (Figure 4F and Videos S6–S8). Taken together, these observations suggested that MTs in P0 and P1c$^{-/-}$ keratinocytes, although growing faster, were less frequently undergoing disassembly and thus overall were less dynamic and consequently more stable compared with their wild-type counterparts.

P1c deficiency affects shape and directional migration of cells

We have previously shown that primary and immortalized P0 keratinocytes migrate with higher velocities than their wild-type counterparts (Osmanagic-Myers *et al.* 2006). Further, it is known that polarized migration of mammalian cells requires stabilized MTs at the cell cortex (for reviews, see Watanabe *et al.*, 2005; Kaverina and Straube, 2011). This prompted us to investigate a possible link between P1c-modulated MT dynamics and cellular features determining the shape and polarity of cells. Seeded at low densities to enable single-cell monitoring,

P1c$^{-/-}$ primary keratinocytes showed a reduction in size (cell area) but an increase in their perimeter compared with wild-type cells (Figure 5, A and B, graphs a and b); P0 cells, too, showed a reduction in size, but hardly a perimeter change. This suggested that primary P1c$^{-/-}$ keratinocytes were displaying more protrusions than wild-type and P0 cells. Accordingly, a statistical analysis of calculated shape factors (SF = $4\pi \times$ area/perimeter^2) and aspect ratios (AR = shortest diameter/largest diameter) revealed wild-type and P0 keratinocytes to be similar in shape, but P1c$^{-/-}$ cells to have more protrusions and to be much more elongated (Figure 5, A and B, graphs c and d).

Time-lapse microscopy of single cells showed that primary P1c$^{-/-}$ keratinocytes migrated faster (~1.0 µm/min) compared with wild-type cells (~0.8 µm/min), albeit still more slowly than P0 cells (~1.2 µm/min; Figure 5B, graph e). One explanation why P1c$^{-/-}$ cells did not reach the velocity of P0 cells could have been that they were still expressing isoform P1a and thus were able to form intact hemidesmosomes that were pinning them down, contrary to P0 cells, which were lacking both isoforms. Interestingly, P1c$^{-/-}$ keratinocytes also showed a drastic loss of directional migration potential compared with wild-type and P0 cells (Figure 5, A, migration tracks, and B, graph f). Promotion of migration through stabilized MTs and simultaneous retention of cells via P1a anchorage, leading to the extreme elongation of cells and loss of directional migration potential, could again be the reason why P1c-deficient but not P0 cells showed this phenotype.

Lack of plectin causes alterations in FA dynamics

To explore possible mechanisms underlying the higher migration rate of plectin-deficient keratinocytes, we examined whether the greater stability of MTs in the mutant cells could compromise the stability of FAs. MT targeting events to FAs have been shown to induce the dissociation of the latter by delivering FA-relaxing factors and promoting FA turnover (for review, see Kaverina *et al.*, 2002). Accordingly, one may expect that the increased number of stable MTs encountered in peripheral cytoplasmic regions of mutant keratinocytes leads to a higher number of MTs converging at peripheral FAs, with consequences for their turnover and size. For analysis of FA turnover, immortalized wild-type and P0 keratinocytes, as well as primary P1c$^{-/-}$ keratinocytes, were transfected with an EGFP-tagged version of the FA marker paxillin (Rottner *et al.*, 2001) and subjected to time-lapse microscopy. Compared with EGFP-paxillin–transfected wild-type keratinocytes, P0 and especially P1c$^{-/-}$ cells displayed smaller FAs (Figure 6A). In addition, when EGFP-paxillin–labeled FAs were monitored over time, their size reduction rate was faster in P0 compared with wild-type cells, while they were hardly showing alterations in size in P1c$^{-/-}$ cells (Figure 6A, graph). To assess whether these differences were related to the frequency of FA targeting by MTs, we analyzed the proportions of MT-targeted versus nontargeted FAs in all three cell types by double staining for tubulin and paxillin (Figure 6B). The quantitative analysis revealed an up to twofold higher level of tubulin and paxillin colocalization at FAs (Figure 6B, arrowheads) in mutant (P1c$^{-/-}$ and P0) versus wild-type cells. Comparable results were obtained using vinculin as an FA marker (unpublished data). Thus those cell types that showed a higher proportion of MT-targeted FAs were also the ones displaying more stable MTs. Moreover, the smaller size of FAs in mutant cells correlated with their higher frequency of being targeted by MTs.

P1c deficiency leads to alterations in glucose uptake, aberrant mitotic spindles, and diminished growth rate of keratinocytes

In additional experiments aimed at establishing the physiological significance of plectin-modulated MT regulation, we measured glucose uptake, spindle formation, and growth rates of mutant (P1c$^{-/-}$ and P0) and wild-type keratinocytes. Glucose uptake is known to involve MT-dependent glucose transporter recycling (Fletcher *et al.*, 2000; Zaid *et al.*, 2008). When keratinocytes were incubated with 2-[N-(7-nitrobenz-2-oxa-1,3-diazol-4-yl)amino]-2-deoxy-D-glucose (2-NBDG), a fluorescent derivative of D-glucose (Yamada *et al.*, 2000), and fluorescence intensities were measured by confocal microscopy, a significantly higher uptake of 2-NBDG by P1c$^{-/-}$ (~2.2-fold) and P0 (~1.5-fold), compared with wild-type cells was observed (Figure 7A). Control experiments performed in the presence of the MT assembly blockers nocodazole (Figure 7A), or colchicine (Figure S4) revealed a dramatic reduction in fluorescence intensity, confirming that 2-NBDG uptake was MT-dependent. Thus a more efficient (MT-dependent) vesicular delivery of glucose transporters could readily explain the increase in glucose uptake shown by P1c$^{-/-}$ and P0 keratinocytes. Indeed, when cells were immunolabeled for GLUT1, and the intensities of GLUT1-specific signals were quantified, a ~4.5 times higher level of glucose transporters was measured for P0 compared with wild-type keratinocytes (Figure 7B).

As MTs are key players in cell division, we investigated whether their stabilization in P1c$^{-/-}$ keratinocytes affects the division process of these cells. Interestingly, the immunostaining of P1c$^{-/-}$ primary keratinocyte cultures using antibodies to α-tubulin, revealed a significant number of aberrant—multipolar and asymmetric—mitotic spindles (Figure 7C). A comparative quantitative analysis of aberrant mitotic spindles observed in P1c$^{-/-}$ and wild-type primary keratinocytes showed an unexpectedly high fraction (40%) of P1c$^{-/-}$mitotic cells to display multipolar or asymmetric spindles, compared with only ~3% of mitotic wild-type cells (Figure 7C, bar graph). The impairment of normal mitotic spindle formation correlated with a substantial delay in the growth rate of P1c$^{-/-}$ compared with wild-type primary keratinocytes over the first 96 h after seeding of the cells (Figure 7D). A similar phenotype has already been observed in P0 fibroblasts (Spurny *et al.*, 2008). Although the molecular mechanism underlying P1c's engagement in mitotic spindle formation awaits elucidation, it is worth noting that plectin has been identified as a component of the mitotic spindle in several proteomic studies focused on the characterization of spindle-associated proteins (Mack and Compton, 2001; Sauer *et al.*, 2005; Gache *et al.*, 2010) and the spindle phosphoproteome (Dephoure *et al.*, 2008; Malik *et al.*, 2009).

P1c antagonizes MAP-mediated MT stabilization

Previous solid-phase binding studies had revealed binding of full-length (rat glioma C6 cell) plectin to high-molecular-weight (HMW) MAPs purified from brain (Herrmann and Wiche, 1987). Thus, in investigating the molecular mechanism underlying P1c-mediated MT destabilization, we first determined, using similar assays, which molecular domain(s) of plectin were involved in MAP binding. Using various fragments of P1c, expressed as fusion proteins with N-terminal glutathione *S*-transferase (GST) tags (Figure 8A), we found that those containing the central part of plectin's N-terminal plakin domain preceding the rod (p1c-30, p16-24, and p20-21), showed binding to at least one of the HMW MAPs (Figure 8B). The minimal fragment showing MAP binding, p20-21, corresponded to plectin's putative SH3 domain (Ortega *et al.*, 2011), raising the possibility that plectin bound to MAPs via this domain. A similar type of interaction has previously been shown for tau, another major MAP, which binds to the SH3 domain of the nonreceptor tyrosine kinases Fyn and Src (Lee *et al.*, 1998). P1c-MAP binding was further demonstrated by cosedimentation of HMW MAPs with P1c pulled down

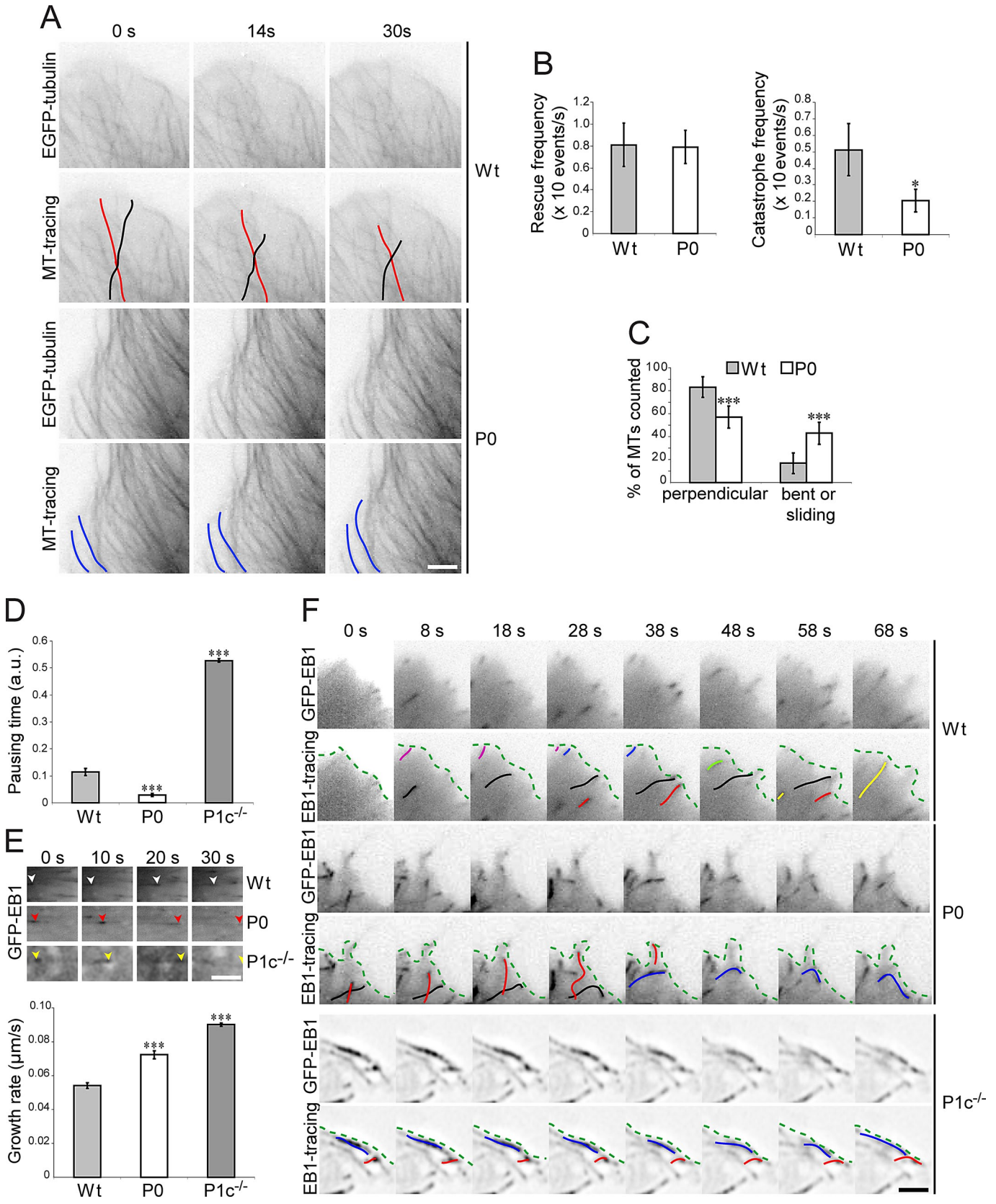

FIGURE 4: P1c affects dynamic properties of MTs. (A) Images taken from a time-lapse recording (Video S1) of immortalized wild-type and P0 keratinocytes transfected with EGFP-tubulin and outlining (MT-tracing) of representative MTs. MTs outlined in red and black denote two examples of shrinking MTs in a wild-type cell, while lines in blue represent MTs in a P0 cell that failed to undergo catastrophe after reaching the membrane. Scale bar: 5 µm. (B) Bar graphs showing analyses of rescue and catastrophe frequencies ($n = 3$; >10 cells/experiment). Error bars: ± 95% CI. *, $p < 0.05$. (C) Graph

from mouse brain lysates using anti-P1c isoform-specific antibodies and protein G–coated beads (Figure 8C).

To establish whether results obtained with MAPs generally considered to be typical for neural cells could be extrapolated to the situation prevailing in keratinocytes, we analyzed whether proteins of the MAP2/tau protein family were expressed at all in mouse epithelial cells. To analyze tau and MAP2 mRNA expression, we subjected total RNA isolated from primary keratinocytes, immortalized keratinocytes, and epidermal tissue to RT-PCR analysis. Using primers binding to sequences in exons 9 and 11 (flanking the second MT-binding domain repeat-encoding exon 10) of the tau gene (Poorkaj *et al.*, 2001; Andreadis, 2005), we found a DNA fragment of the expected size (390 base pairs; Duff *et al.*, 2000) was amplified in all cases, including adult mouse brain RNA run as positive control (Figure 8D). DNA sequencing of the PCR products confirmed that they had been derived from tau transcripts. To detect MAP2 transcripts, we used primers binding to sequences in exons 5 and 6, which are common to all MAP2 splice variants (Dehmelt and Halpain, 2005). Single bands of the expected size (344 base pairs) were amplified from all tissues analyzed, including the positive control. Among the samples analyzed, the immortalized mouse keratinocyte cell line has been shown to be devoid of any contaminating fibroblasts or melanocytes (Osmanagic-Myers *et al.*, 2006), so these data unambiguously demonstrated that tau and MAP2 mRNAs are expressed in mouse keratinocytes. To examine whether tau and MAP2 are also expressed on the protein level in skin, we subjected frozen foot pad skin sections from adult mice to IFM. Using antibodies specific to tau or to MAP2, we detected a pronounced, predominantly cytoplasmic staining of all live epidermal keratinocyte cell layers (Figure 8E). Similar staining patterns were observed on sections from other skin areas, such as ear and tail skin (unpublished data). Controls not using primary antibodies were negative (Figure 8E).

To better understand the molecular mechanism involved in MT destabilization through plectin, we first studied the effects of plectin's SH3 domain on MAP-promoted in vitro assembly of tubulin into MTs. For these assays, we used MAP-free tubulin, along with fragments p20-21 corresponding to plectin's SH3 domain and recombinant MAP2c. On incubation of MAP-free tubulin with MAP2c, under conditions in which tubulin itself polymerized only poorly (if at all), ~65% of the tubulin was found to form polymers in the absence of fragment p20-21 (Figure 9A, lane 4). When increasing concentrations of fragment p20-21 were mixed with MAP2c prior to induction of MT formation, increasing amounts of MAP2c were found in the soluble fractions, indicating reduced MT binding of MAP2c in the presence of fragment p20-21. Ultimately, reduced MAP2c binding to MTs led to a shift of tubulin from the insoluble to the soluble fraction, indicating an inhibition of MAP2c-promoted MT assembly. To confirm these data, we carried out a similar experiment using a fragment of plectin (p16-21) containing not only the SH3 domain, but also the preceding sequences corresponding to plectin's spectrin repeats 4 and 5. In this case, the observed suppression of MAP2c-promoted MT assembly was even stronger (Figure S5A). The higher efficiency of this fragment in inhibiting MAP2c-mediated MT stabilization could be a result of improved structural folding of the SH3 domain by intramolecular interaction with spectrin repeat 4 (Ortega *et al.*, 2011). In fact, circular dichroism (CD) measurements of fragment p16-21 revealed a well-defined α-helical structure of the protein in solution (Figure S5B), whereas fragment p20-21 (corresponding to the SH3 domain without spectrin repeats) appeared to be intrinsically disordered (unpublished data) and was expected to assume a folded structure only upon interaction with MAPs.

To assess whether fragment p20-21 could compete with MTs for tau binding under conditions in which the polymeric state of MTs was maintained (i.e., without disassembly of the polymer), we incubated increasing concentrations of fragment p20-21 with brain lysates containing polymerized MTs under conditions favoring the polymerized state of MTs even after removal of MAPs (for details, see *Materials and Methods*). The analysis of polymeric MTs (i.e., sedimentable by high-speed centrifugation) and their coassembling (bound) proteins by IB revealed a decrease in MT-bound tau protein with increasing concentrations of fragment p20-21 (Figure 9B). These data, similar to those obtained using purified recombinant MAP2c (Figure 9A), were consistent with the notion that plectin's SH3 domain could bind to and thereby prevent the interaction of MAPs with tubulin.

On the basis of these in vitro results, one may have expected higher levels of MAPs to be bound to MTs in plectin-deficient compared with plectin-positive cells. For an investigation of this idea, wild-type, P1c$^{-/-}$, and P0 primary keratinocytes were triple-immunostained using antibodies to MAP2, α-tubulin, and P1c. While MAP2 showed a dotted staining pattern along MTs in wild-type keratinocytes (Figure 9C, top panels), MTs were decorated with MAP over much longer distances in both of the mutant cell types (Figure 9C, arrowheads). However, in contrast with P1c$^{-/-}$ keratinocytes, P0 cells showed MAP2 signals associated not only with MTs but also

represents proportions (%) of MTs in wild-type vs. P0 cells that were growing perpendicularly toward the plasma membrane (without bending) or bending and/or sliding along the membrane ($n = 3$; 10 cells/experiment). Error bars: ± 95% CI. ***, $p < 0.001$. (D) Bar graph representing the pausing times of EB1 comets measured in wild-type, P0, and P1c$^{-/-}$ keratinocytes normalized to the total time of MT growth recorded. Error bars: ± SEM. ***, $p < 0.001$. (E) Time-lapse images (Video S5) of selected single EB1 comets continuously growing (without pausing) between time points measured; representative examples for wild-type, P0, and P1c$^{-/-}$ cells are shown. Note faster growth of EB1 comets (corresponding to growing tips of MTs) in both types of mutant cells (red and yellow arrowheads) compared with their wild-type counterpart (white arrowheads) over the same time period. Scale bar: ~3 µm. Graph shows analysis of MT growth rates ($n = 3$; ~20 cells/experiment). Error bars: ± 95% CI. ***, $p < 0.001$. (F) Single-frame images taken from time-lapse recordings of GFP-EB1–expressing immortalized wild-type and P0, as well as primary P1c$^{-/-}$ keratinocytes (Videos S6–S8, respectively. Note that Videos S6–S8 show details of Videos S2–S4). Colored lines mark trajectories of different EB1 comets (EB1-tracing). Green broken lines mark cell margins. Colored EB1 traces in wild-type images (top rows) represent individual MTs that grow toward the periphery and disappear after reaching the margin; outlined trajectories in P0 cells (middle rows) mark MTs that continue to grow upon reaching the membrane and either meander (red line) or bend and grow parallel to the membrane (blue and black lines); EB1 traces in P1c$^{-/-}$ images (bottom rows) show MTs that continuously grow along the membrane, and MTs that bend and keep growing after reaching the membrane. Scale bar: 5 µm. Note that a different microscopy setup was used for the imaging of wild-type and P0 cells than for imaging of P1c$^{-/-}$ cells (see *Materials and Methods*).

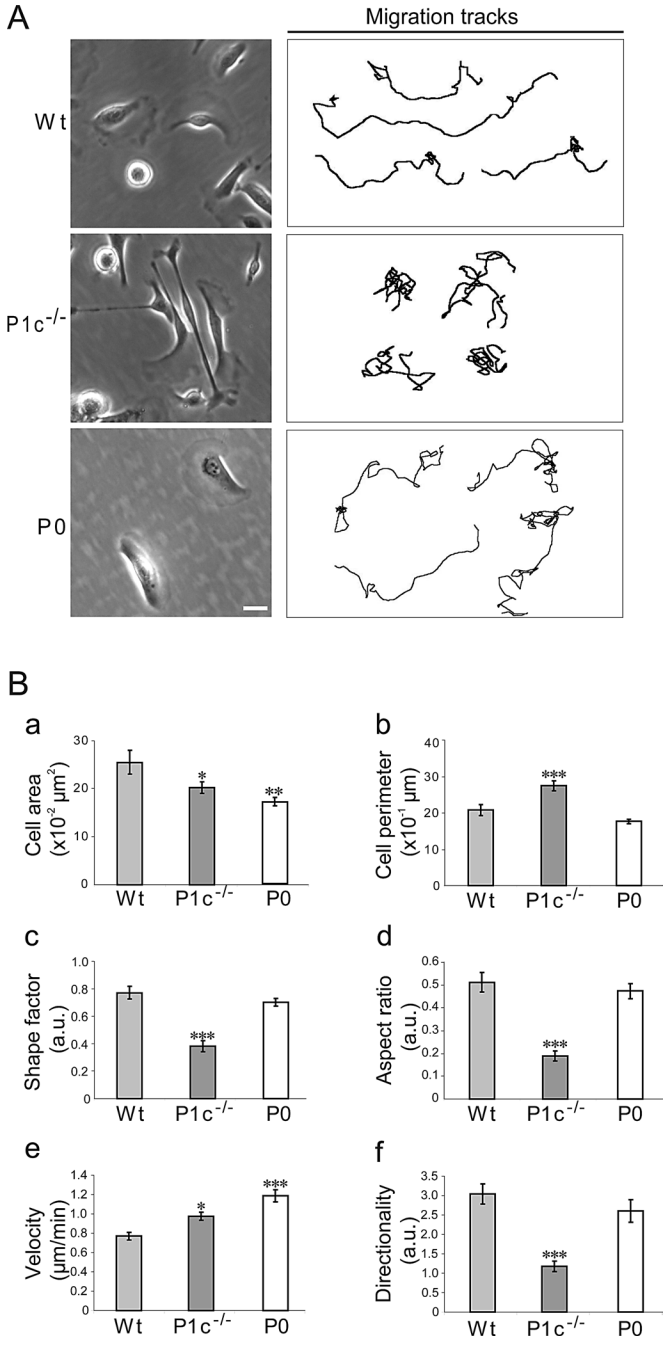

FIGURE 5: Alterations in shape and polarized migration of P1c-deficient keratinocytes. (A) Phase-contrast images of representative primary wild-type, P0, and P1c$^{-/-}$ keratinocytes and migration traces of single cells (monitored by video microscopy) are shown. Scale bar: 100 µm. (B) Bar graphs show statistical analyses of cell area (a), cell perimeter (b), shape factor (c), aspect ratio (d), velocity (e), and directionality (f) of migrating primary wild-type, P1c$^{-/-}$, and P0 keratinocytes ($n = 3$; 20 cells/experiment). *, $p < 0.05$; **, $p < 0.005$; ***, $p < 0.001$.

with structures without apparent linkage to MTs. Accordingly, a quantitative evaluation of MAP–MT colocalization revealed a ~1.8 times higher value for P1c$^{-/-}$ than for P0 cells. The lower level of MT-bound MAPs in P0 compared with P1c$^{-/-}$ cells could be due to the elevated basal activities of Src and Erk1/2 MAP kinases known to prevail in these cells (Osmanagic-Myers *et al.*, 2006), as both activities have been shown to act as regulators of MAP–MT binding (Lim and Halpain, 2000; Lee, 2005).

DISCUSSION

Based on three types of assays—resistance to MT-depolymerizing drugs, assessment of acetylated tubulin levels, and direct observation of MT dynamics by video microscopy—our study provides evidence that P1c deficiency in keratinocytes results in increased MT stability. This increased stability was coupled with a decrease in the dynamics of MTs, manifesting as less frequent transitions between MT assembly and disassembly states. A destabilizing function of this kind was not expected for a cytolinker protein such as plectin and, in fact, it was the opposite of what had been observed for other cytolinkers, such as ACF7 and BPAG1, which have been shown to stabilize MTs (Kodama *et al.*, 2003; Yang *et al.*, 1999). Thus plectin seems to be the first cytolinker protein shown to act as an MT destabilizer. This finding, together with the observation that plectin can act also as a destabilizer of the actin cytoskeleton (Andrä *et al.*, 1998), opens a new perspective on how cells maintain their cytoskeletal integrity. We show that this process is the result of a fine-tuned regulatory mechanism, in which cytolinker proteins are key players, not only anchoring and providing stability to dynamic filaments but also destabilizing them and thus favoring their dynamic behavior, as demonstrated in this study for P1c.

Our study demonstrates that abnormal MT stability in P1c$^{-/-}$ keratinocytes could be rescued, that is, restored to normal levels, using P1c-EGFP fusion proteins. However, from experiments in which we transfected P1c$^{-/-}$ keratinocytes with truncated forms of P1c lacking the IF-binding domain, evidence emerged that the rescue potential of P1c was dependent on the localization of the protein, in particular its association with IFs. Unable to be recruited to IF networks, and instead associating with actin filaments, these truncated versions showed only limited, if any, rescue potential. These findings point toward a fascinating new feature of cytoskeletal filament cross-talk, namely, the potential of IFs to destabilize MTs via an associated cytolinker protein, thereby stimulating MT dynamics.

As a possible mechanism underlying MT destabilization through plectin, we suggest that plectin's SH3 domain interferes with MAP–MT binding and consequently antagonizes MAP-mediated MT stabilization (Figure 9D). Several observations support such a mechanism. First, using expression constructs encoding various domains of plectin, we could show that plectin's SH3 domain is responsible for plectin's binding to HMW MAPs, an interaction reported years ago (Herrmann and Wiche, 1987). Second, MT coassembly assays demonstrated that increasing concentrations of recombinant versions of plectin's SH3 domain, or fragments of plectin containing it, led to diminished levels of MAPs binding to MTs and, as a consequence, fewer polymerized MTs. Third, on the basis of an endogenous tau–MT binding assay, we could show that plectin's SH3 domain was able to detach MAPs from stabilized MTs present in brain tissue lysates. Fourth, comparing in situ MAP–MT decoration in wild-type, P1c$^{-/-}$, and P0 keratinocytes, MAP2 was found to be associated with larger portions of cellular MTs in mutant compared with wild-type cells (in which P1c's presence interferes with MAP–MT binding).

Our finding that MAP2 and tau are expressed in nonneuronal cells and tissues, such as mouse keratinocytes and epidermis, is not unprecedented. Early on, expression of MAP2 isoforms could be detected in skeletal muscle, heart, kidney, and tracheal epithelium, as well as in human skin fibroblasts and CHO cells (Wiche *et al.*, 1984), and, confirming these findings, MAP2 protein was identified also in the human HaCaT keratinocyte cell line (Liu *et al.*, 2007).

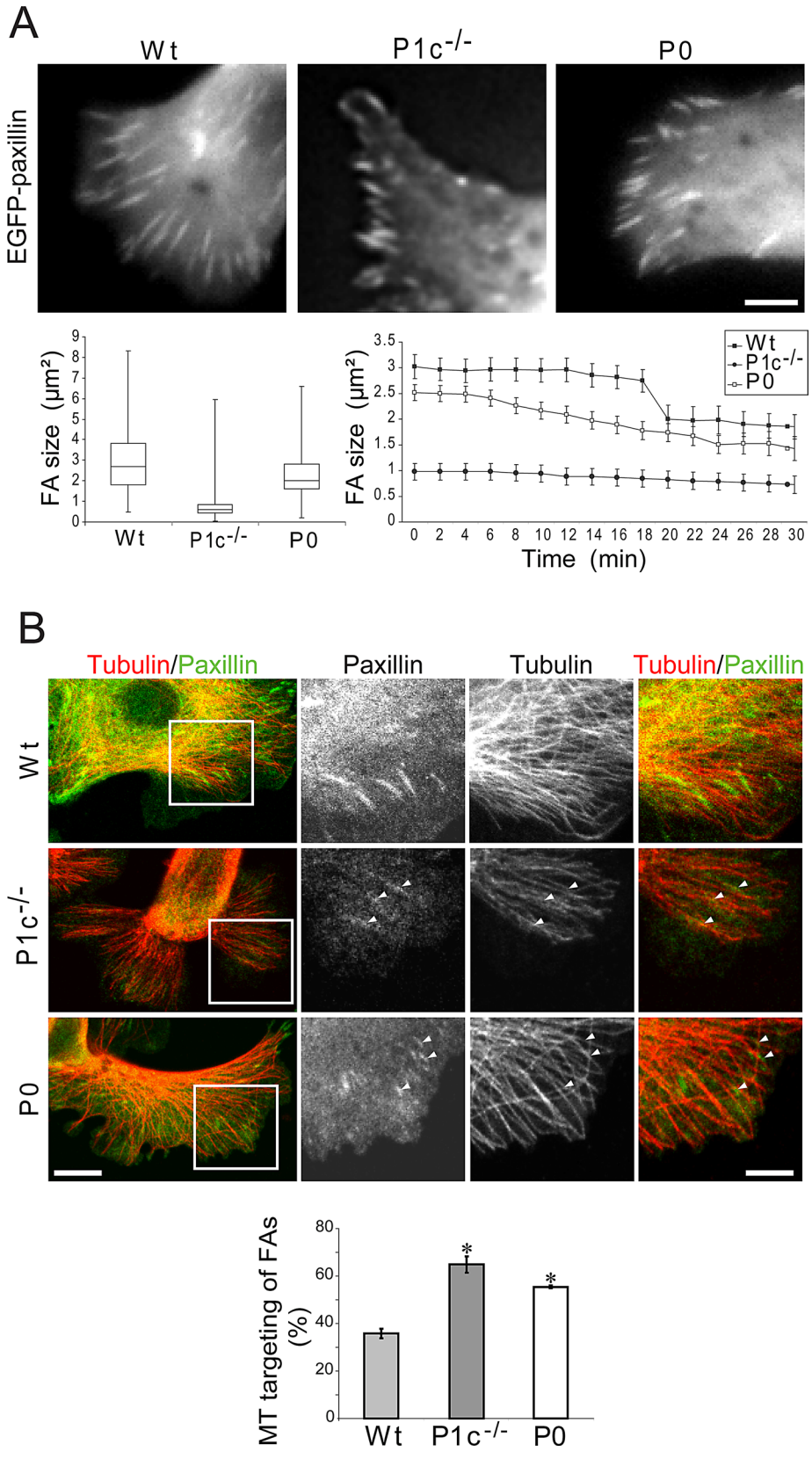

FIGURE 6: Loss of P1c alters FA dynamics. (A) Images of EGFP-paxillin–expressing immortalized wild-type and P0 and primary P1c$^{-/-}$ keratinocytes. Scale bar: 10 µm. Box-and-whisker plots indicate the median (middle line in the box), 25th percentile (bottom line of the box), 75th percentile (top line of the box), and 2.5th and 97.5th percentiles (whiskers) of FA size values. Graph shows changes in FA size over time ($n = 3$; 10 cells/experiment). Error bars: ± SEM. (B) Cells as in (A) double immunolabeled using antibodies to paxillin (green) and α-tubulin (red) to distinguish between MT-positive (arrowheads) and MT-negative FAs. Left column shows survey views of wild-type, P1c$^{-/-}$, and P0 keratinocytes. Scale bar: 10 µm. The three columns on the right show selected views (boxed) in detail. Scale bar: 5 µm. Bar graph: statistical analysis of MT-targeting of FAs in wild-type and mutant keratinocytes evaluated by a chi-square test ($n = 3$; 10 cells/experiment). *, $p < 0.05$. Error bars: ± SEM.

Furthermore, the expression of various tau isoforms has also previously been detected in different nonneuronal cell types and tissues, including kidney, skeletal muscle, heart, lung, breast epithelium, and pancreatic acinar cells (Gu *et al.*, 1996; Vanier *et al.*, 1998; Rouzier *et al.*, 2005).

Because plectin's SH3 domain is expressed in all of its known isoforms and SH3 domains are contained in many other proteins, including regulators of MAPs, such as the kinases Fyn and Src (Lee *et al.*, 1998; Lim and Halpain, 2000), SH3 domain-mediated MT destabilization could be a function performed by plectin isoforms other than P1c, as well as by other proteins. However, at least for the cases of the signaling proteins Src and Grb2, it has been shown that their SH3 domains, in contrast to plectin's SH3 domain, bind only to the MT-unbound fraction of MAPs (Lim and Halpain, 2000), suggesting that these proteins are not directly involved in regulating MT dynamics, but rather in trafficking of MAPs (Usardi *et al.*, 2011; Pooler *et al.*, 2012). Although all plectin isoforms have the potential to destabilize MTs via their SH3 domain, P1c is likely to be more efficient than other isoforms, due to its closer apposition to the MT surface, which is effected by an additional tubulin-binding interface formed by its isoform-specific N-terminal sequence and the succeeding ABD (R.G.V., L.J., and G.Wi., unpublished data). The partial cosedimentation of endogenous keratinocyte P1c (but not P1a) with MTs observed in our study supports this notion. A weak or even only transient binding of P1c to tubulin polymers might suffice to bring plectin's SH3 domain in contact with MAPs.

As depicted in the working model shown in Figure 8D, we propose that, by antagonizing MAP-mediated MT stabilization, IF-associated P1c leads to a MT network that is more susceptible to localized disassembly in the vicinity of IFs. Conversely, in a plectin-deficient system, the fraction of MAPs attaching along MTs is higher, leading to promotion of assembly and stabilization of the polymer. This model does not exclude additional or alternative ways of how plectin

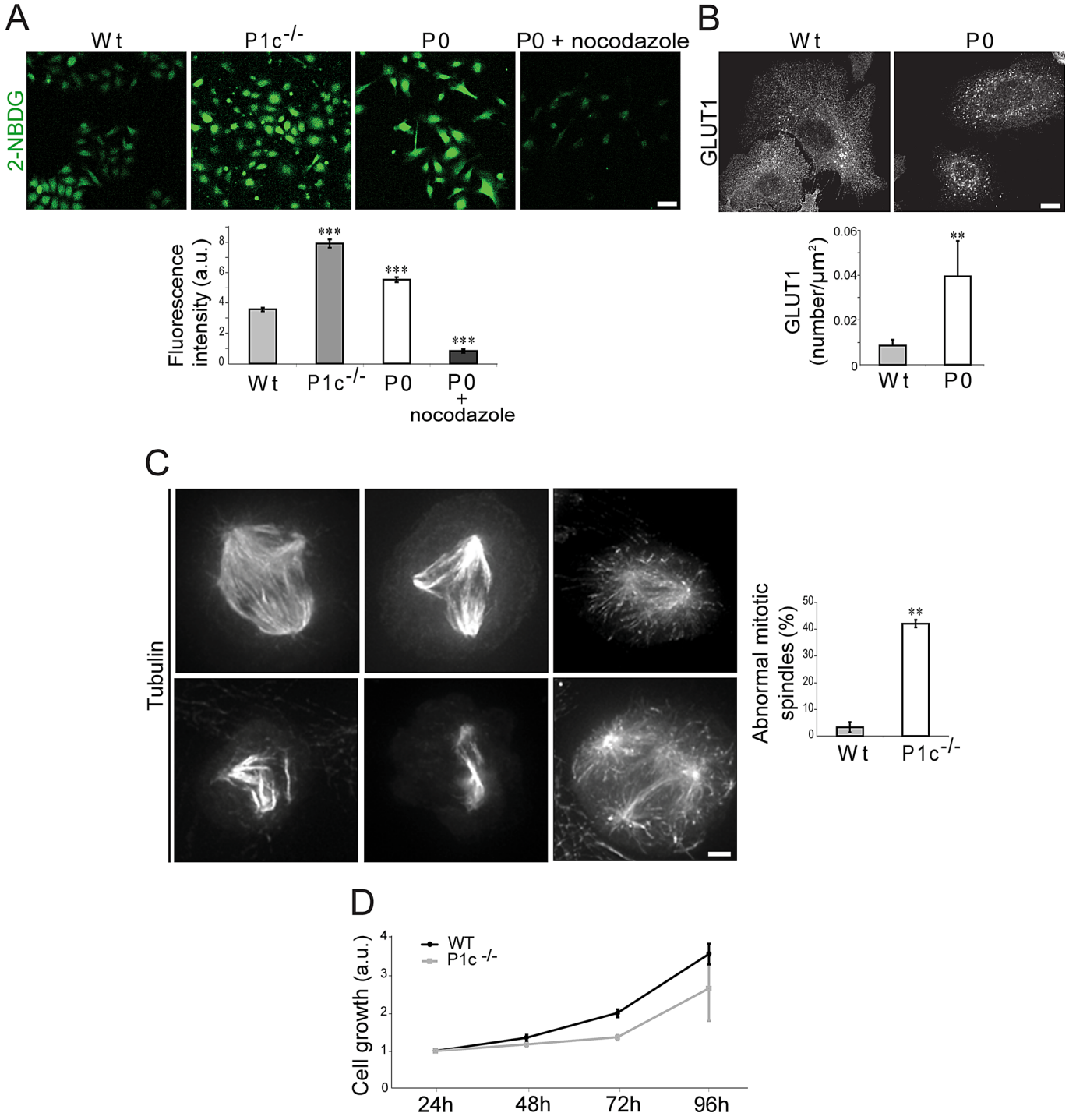

FIGURE 7: Alterations of glucose uptake and mitotic spindle formation in plectin-deficient keratinocytes. (A) Primary wild-type, P1c$^{-/-}$, P0, and nocodazole-treated P0 keratinocytes were incubated with 2-NBDG, and fluorescence intensities of cells were measured. Data were evaluated as described in the text ($n = 3$; 200 cells/experiment). ***, $p < 0.001$. Error bars: ± 95% CI. Scale bar: 1 mm. (B) Quantification of GLUT1 by immunolabeling of keratinocytes using antibodies to GLUT1. Scale bar: 10 μm. Bar graph represents GLUT1 signals normalized to total cell area ($n = 3$; 10 cells/experiment). **, $p < 0.01$. Error bars: ± 95% CI. (C) Gallery of abnormal mitotic spindle formations in primary P1c$^{-/-}$ keratinocytes. Spindle apparatuses were visualized by immunolabeling using antibodies to α-tubulin. Scale bar: 10 μm. Bar graph shows evaluation of abnormal mitotic spindles ($n = 4$; ~150 cells/experiment). **, $p < 0.01$. Error bars: ± 95% CI. (D) Growth rates of primary wild-type and P1c$^{-/-}$ keratinocytes measured during 96 h after seeding ($n = 3$). Error bars: ± SEM.

may participate in MT dynamics (e.g., through its scaffolding and platform function for other putative MT regulators).

Previous studies revealed plectin not only as a cytolinker providing stability against mechanical stress, but also as a scaffolding and signaling platform able to mediate cellular stress responses (Gregor *et al.*, 2006; Osmanagic-Myers *et al.*, 2006). Our study adds another interesting aspect to this scenario by unmasking P1c as an MT destabilizer and showing that cytolinker-mediated MT destabilization

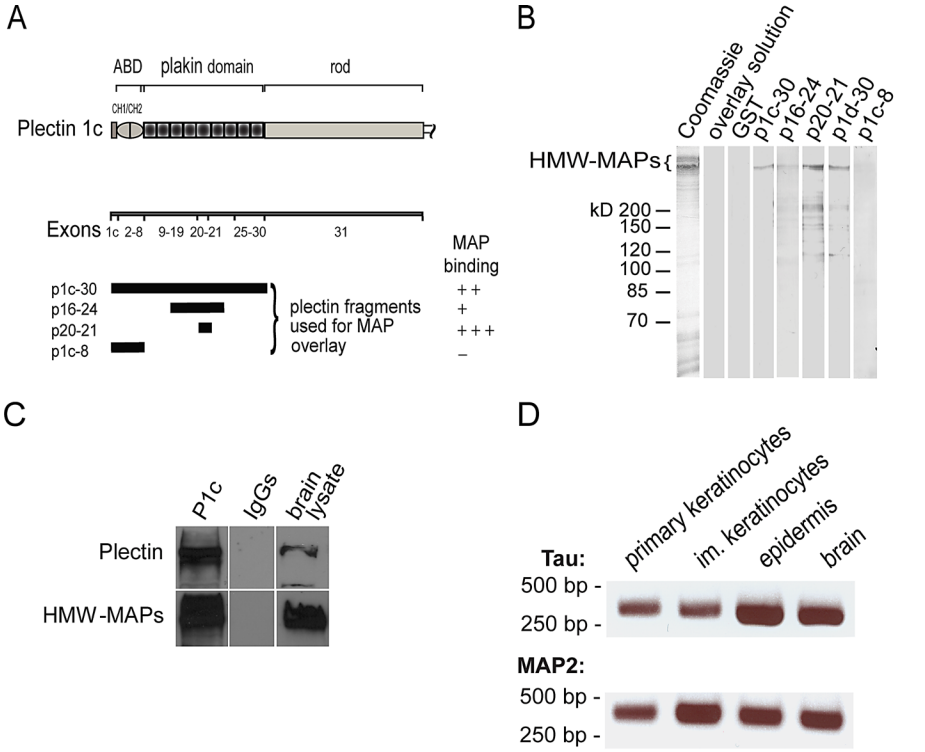

FIGURE 8: P1c-MAP interaction and expression of tau and MAP2 in cultured keratinocytes and epidermis. (A) Scheme of N-terminal subdomains, exon allocations, and fragments of plectin used for overlay assays. (B) Overlay assay showing binding of N-terminal plectin fragments to HMW MAPs. Note strongest signal observed with p20-21. Semi-quantitative estimates of MAP-binding affinities obtained by densitometric scanning of gels are indicated in (A). (C) Coimmunoprecipitation of endogenous HMW MAPs with P1c from brain lysates. Note that P1c and HMW MAPs showed cosedimentation when anti-P1c antibodies were used, but not when nonspecific IgGs were used ($n = 3$). (D) Tau and MAP2-specific cDNA fragments amplified from total RNA contained in cell lysates of primary and immortalized keratinocytes, epidermis, and brain, using RT-PCR (primers are specified in Table S1); brain was used as positive control for tau and MAP2. (E) IFM of frozen foot pad skin sections from adult wild-type mice using antibodies to tau or MAP2. In negative controls, primary antibodies were omitted; nuclei were stained with 4′,6-diamidino-2-phenylindole. Note relatively strong immunofluorescence signals for both antigens in epidermis (e), and weaker signals in hair follicles (asterisk) and in a few scattered cells in the dermis (d). Scale bars: 25 μm.

is required for the correct performance of multiple physiological processes. We demonstrate that P1c deficiency in keratinocytes leads to alterations in shape and polarized migration of cells, and that the more stable MT network in P1c$^{-/-}$ keratinocytes makes the cells migrate faster, due to more protrusion at the cell periphery and a higher FA turnover rate. Moreover, we show that increased MT stability in the absence of plectin results in elevated glucose uptake, due to accumulation of glucose transporters at the membrane, and we demonstrate that the formation of aberrant mitotic spindles leads to alterations in cellular growth rates. No other cytolinker protein has been reported to affect cellular functions of such a broad spectrum. This makes P1c not only a uniquely versatile plectin isoform but also an essential element in the orchestration and correct functioning of MT-dependent cellular processes.

In view of plectin's widespread expression and distinct cellular localization of its isoforms, we expect the newly identified function of plectin as an MT assembly antagonist to play a role in various other cell systems. Of particular interest for future studies are cells of the central and peripheral nerve systems, which express P1c at high levels and in which the dynamic behavior of MTs is an essential feature of proper cell performance.

MATERIALS AND METHODS

cDNA constructs

Mammalian expression plasmids encoding GFP-EB1 (Stepanova *et al.*, 2003), EGFP-tubulin and EGFP-paxillin (Rottner *et al.*, 2001), and the bacterial expression plasmid pET3d/MAP2c encoding rat MAP2c (Ludin *et al.*, 1996) were kindly provided by A. Akhmanova (Erasmus Medical Center, Rotterdam, The Netherlands), J. Wehland (Gesellschaft für Biotechnologische Forschung, Braunschweig, Germany), and A. Matus (Friedrich Miescher Institute, Basel, Switzerland), respectively. Mammalian expression plasmids encoding full-length mouse P1c and P1c-8 with C-terminal EGFP have been described previously (Rezniczek *et al.*, 2003); expression plasmid P1c-30 with C-terminal EGFP was prepared similarly. Plectin cDNA fragments corresponding to exons 1c–8 (p1c–8, aa 1–299, NCBI Reference Sequence: NP_035247); exons 1c–30 (p1c–30, aa 1–1374); exons 16–24 (p16–24, aa 632–1018); exons 20–21 (p20–21, aa 815–889) were excised from existing plasmids (constructed as described in Rezniczek *et al.*, 2003), and inserted into the *Eco*RI site of the bacterial expression vector pGEX-4T-1 (GST gene fusion system). The plectin fragment corresponding to exons 16–21 (aa 642–917) was cloned into a modified version of bacterial expression vector pETM60.

Antibodies

The following primary antibodies were used for IFM, IB, and immunoprecipitation (IP): affinity-purified isoform-specific rabbit antisera to P1c and P1a (IFM, IB, IP; Rezniczek *et al.*, 1998; Andrä *et al.*, 2003), rabbit antiserum to MAP2 (IFM, IB; Wiche *et al.*, 1983), rabbit antiserum PRB-160P to keratin 5 (IFM; Covance, Princeton, NJ), mouse mAb T5168 to α-tubulin (IFM, IB; Sigma-Aldrich, St. Louis, MO), rabbit antiserum to tau (IB; Dako, Carpinteria, CA), mouse mAb to neurofilament 160 kDa (IB;

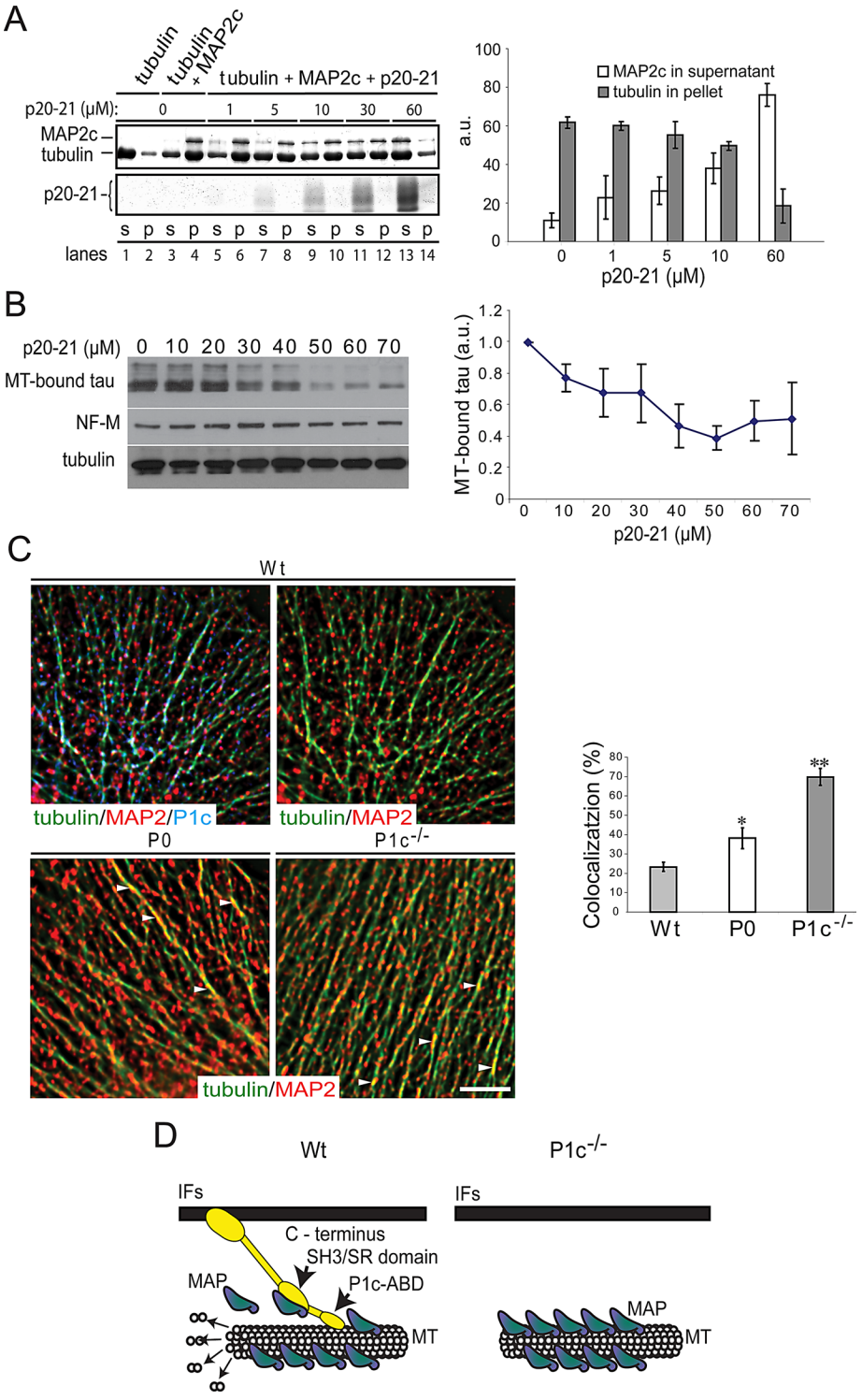

FIGURE 9: Plectin's SH3 domain compromises MAP–MT interaction. (A) Inhibition of MAP2c promoted in vitro assembly of MTs by fragment p20-21. MTs were assembled in vitro from purified samples of tubulin and recombinant MAP2c in the presence of fragment p20-21 (at concentrations indicated) and sedimented by centrifugation. Resulting pellet (p) fractions (containing polymerized MTs and MT-bound MAP2c), and supernatant (s) fractions (containing soluble tubulin and unbound MAP2c, as well as p20-21) were analyzed by SDS–PAGE. Coomassie blue–stained gel bands corresponding to MAP2c and tubulin in s and p fractions were quantified (bar graph). Error bars: ± SD ($n = 5$). (B) Disruption of tau–MT interaction by fragment p20-21. The detachment of endogenous tau from stabilized MTs (contained in brain cell lysates) was measured by SDS–PAGE of sedimented MT fractions after incubation of lysates with p20-21 at concentrations indicated. Coomassie blue–stained protein bands corresponding to MT-bound tau, sedimented tubulin (MT polymers), and neurofilament protein M (NF-M; loading control) are shown. Quantification (graph) as in (A). Error bars: ± SEM ($n = 5$). (C) Deconvolved IFM images of cytoplasmic regions of primary wild-type, P1c$^{-/-}$, and P0 keratinocytes using antibodies as indicated. Arrowheads, patches of MAP2 along MTs. Scale bar: 2 μm. Bar graph, percentages of colocalizing tubulin and MAP2 signals. Error bars: ± SEM ($n = 3$). *, $p > 0.05$; **, $p > 0.01$. (D) Model depicting plectin as MT destabilizer. Binding of P1c to MTs presumably occurs via its isoform-specific N-terminal sequence, including the ABD, while the SH3 domain located within the plakin domain binds to MAPs. Interference with the MT-stabilizing function of MAPs ensures a dynamic MT network in wild-type cells. When P1c is absent, more MAPs can bind along MTs, leading to their stabilization.

Chemicon, Billerica, MA), mouse mAb VIN-11-5 to paxillin (IFM; BD Transduction Laboratories, San Jose, CA), rat mAb SM2202P to α-tubulin (IFM; Acris, Herford, Germany), mouse mAb T6793 to acetylated tubulin (IFM, IB; Sigma-Aldrich), rabbit antiserum to GLUT1 (IFM; Millipore, Billerica, MA), and mouse mAb GST2 to GST (IB; Sigma-Aldrich). Donkey Alexa Fluor 488 anti-rabbit and goat Alexa Fluor 488 anti-mouse immunoglobulin G (IgG; Invitrogen, Carlsbad, CA), and donkey Rhodamine Red anti-mouse, goat Texas Red anti-rat, and horseradish peroxidase (HRP)-conjugated IgGs (all from Jackson ImmunoResearch, West Grove, PA) were used as secondary antibodies. Actin was stained using phalloidin conjugated to Texas Red-X T-7471 (IFM; Molecular Probes, Carlsbad, CA).

Cultivation, drug treatment, and transfection of keratinocytes

Primary keratinocytes isolated from the epidermis of wild-type, P1c$^{-/-}$, and P0 mice, and immortalized (p53$^{-/-}$) wild-type and P0 keratinocyte cell lines were cultivated as described previously (Osmanagic-Myers *et al.*, 2006; Andrä *et al.*, 2003). For assessment of MT stability, cells were kept in culture medium supplemented with 1 μM nocodazole (in dimethyl sulfoxide [DMSO]) before being fixed and processed for microscopy. For transient transfection of immortalized cells, FuGENE 6 transfection reagent (Roche, Indianapolis, IN) was used; primary cells were transfected in nucleofection kit solution for human keratinocytes using Amaxa technology (Lonza, Cologne, Germany). All experiments including animals were performed in agreement with Austrian Federal Government laws and regulations.

Measurement of 2-NBDG uptake

Primary mouse keratinocytes were incubated with 600 µM 2-NBDG for 15 min following the protocol described by Yamada *et al*. (2000). Fluorescence intensities of 2-NBDG were collected using a confocal microscope (LSM 510; Zeiss, Jena, Germany) equipped with an Achroplan 20×/0.4 numerical aperture (NA) objective lens. Images were recorded using the LSM 510 module and the LSM software, and after background subtraction, fluorescence intensity was measured using ImageJ software (National Institutes of Health, Bethesda, MD).

IFM and image analysis

Prior to microscopy, cell cultures were rinsed (1 min) with prewarmed (37°C) 60 mM PIPES (pH 6.9), 25 mM HEPES, 10 mM ethylene glycol tetraacetic acid (EGTA), and 2 mM $MgCl_2$ (MT-stabilizing solution). Cells were then fixed with 2.5% paraformaldehyde, permeabilized with 0.1% Triton X-100, and immunolabeled using the antibodies described above (*Antibodies*). Immunolabeled single MTs remaining in nocodazole-treated cells were traced, and their length was measured using LSM software (Zeiss) and normalized to total cell area. The proportion of acetylated to total tubulin in MTs was measured in double-labeled specimens by selecting acetylated tubulin-positive and tubulin-positive areas (in pixels) using the magic wand tool in Adobe Photoshop CS2 (San Jose, CA) and keeping the tolerance constant. Immunolabeled GLUT1 clusters were counted using ImageJ software, and values were normalized to cell area after GLUT1 immunolabeling of keratinocytes.

Time-lapse microscopy

Cells expressing GFP-EB1, EGFP-tubulin, or EGFP-paxillin were kept in a closed POCmini cultivation system (Zeiss), and live-cell imaging was performed using an inverted microscope (Axiovert S100TV; Zeiss) as described previously (Osmanagic-Myers *et al*., 2006), or a DeltaVision Image Restoration microscope system (Applied Precision Instruments, Issaquah, WA). Frames of GFP-EB1 and EGFP-tubulin were collected at 37°C with a Plan-Apochromat 100×/1.4 NA oil-immersion objective lens every 2 s for 5 min; EGFP-paxillin images were acquired every 2 min for 30 min. Individual MTs and FAs were tracked using MetaMorph 6.3 software (MDS Analytical Technologies, Sunnyvale, CA) or Image J software. Migrating keratinocytes were recorded using an AxioObserver Z1 microscope coupled to AxioCam MRm (Zeiss) equipped with phase-contrast optics. Frames were taken at 37°C with an EC Plan-Neofluar 10×/0.3NA objective lens for 7-min intervals over a period of 12 h. Images were processed with Zeiss AxioVision 4.8.1 image analysis software and further analyzed with ImageJ software for manual tracking of migrating cells. For tracking the whole-cell trajectory, cell nuclei were marked for each frame throughout the entire time-lapse sequence.

Confocal laser-scanning and epifluorescence microscopy

Microscopy was performed at room temperature using a confocal laser-scanning microscope (LSM 510; Zeiss) equipped with a Plan-Apochromat 63×/1.4 NA oil-immersion objective lens, or with a DeltaVision Image Restoration microscope system, equipped with a Plan-Apochromat 60×/1.4 NA oil-immersion objective lens. Images were recorded using the LSM 510 module and the LSM software, or deconvolved, and processed with softWoRx software (Applied Precision Instruments). Image acquisition was performed at room temperature for fixed samples embedded in Mowiol. Images were subjected equally across the entire image to a minimum degree of Gaussian filter or histogram stretch.

Affinity isolation of MAPs from cultured cells using preformed MTs

Confluent monolayers of immortalized wild-type keratinocytes were harvested in ice-cold phosphate-buffered saline (PBS), collected by centrifugation at 1000 rpm for 5 min at 4°C, and washed in 140 mM NaCl, 8 mM Na_2PO_4, 1.5 mM KH_2PO_4, 3 mM KCl, 0.5 mM $MgCl_2$, 5.5 mM glucose, 1 mM EGTA, and Complete Mini Protease Inhibitor Cocktail tablets (CMPI; Roche). Cells were then homogenized in 100 mM MES (pH 7.0), 0.5 mM $MgCl_2$, 1 mM EGTA, 1 mM GTP, 520 mM sucrose, 50 mM dithiothreitol (DTT), and CMPI, using a syringe with a 22-gauge needle. After removal of cells and nuclei by centrifugation, the supernatant was retrieved, drawn 10 times through a 27-gauge needle, and subjected to ultracentrifugation (Beckman Tabletop TL-100, Brea, CA) at 45,000 rpm for 90 min at 2°C, to obtain a high-speed supernatant (HS-SN). A measure of 650 µg/ml of preformed Taxol-stabilized MTs (Vallee, 1986) prepared from hog brain tubulin (99.9% pure; Cytoskeleton, Denver, CO) was added to keratinocyte HS-SNs, and incubated for 1 h on ice. MTs and bound proteins were sedimented by centrifugation at 16,000 × *g* for 30 min at 4°C. The sedimented material was washed twice in 100 mM MES (pH 7.0), 1 mM EGTA, 0.5 mM $MgCl_2$, 1 mM GTP, 20 µM Taxol, and CMPI by resuspension and centrifugation, before being subjected to SDS-5% PAGE and IB using anti-P1c and anti-P1a isoform-specific antibodies.

Purification of MAPs from brain and protein overlay assays

MAPs were purified from hog brain and adult mouse brain according to Karr *et al*. (1979) and Shelanski *et al*. (1973), respectively. For overlay assays, hog brain MAPs were separated by SDS-5% PAGE, transferred to nitrocellulose membranes, and overlaid with 8 µg/ml of purified recombinant GST-tagged plectin fragments (Rezniczek *et al*., 2004)

Purification of proteins expressed in bacteria

For expression of recombinant plectin fragments, cDNA constructs were cloned into expression vectors pGEX4-T1 (GST-tag; GE Healthcare, Little Chalfont, England) and expressed in the *Escherichia coli* strain BL21 $(DE3)_{ril}$. GST fusion proteins were purified on glutathione-Sepharose 4B beads as described in the manufacturer's instructions (GE Healthcare). Fragment p16-21 was purified by nickel-chelating affinity chromatography. The ubiquitin fusion protein and the His-tag present at the N-terminus were cleaved off by digestion with tobacco etch virus protease and removed by a second round of nickel-chelating affinity chromatography (Rogov *et al*., 2012). The protein was further purified on a SuperdexTM 75 size-exclusion chromatography column (GE Healthcare). For purification of untagged p20-21 protein, bacterial pellets were resuspended in 50 mM Tris-HCl (pH 7.9), 5 mM EDTA, 1% Triton X-100, and 0.1 mg/ml of lysozyme, and cells were disrupted by three cycles of sonication and centrifugation at 12,000 × *g* at 4°C. In the final round, pellets were resuspended in 50 mM ammonium acetate (pH 3.5). Proteins in the final supernatant were concentrated using an Amicon (Billerica, MA) ultracentrifugal filter unit (5-kDa size-exclusion limit) and purified by fast protein liquid chromatography using a Superdex 75 column (GE Healthcare) equilibrated with citric acid (pH 3.5). For increased solubility, p20-21 fractions were adjusted with NaOH to pH 12.0, centrifuged at 12,000 × *g* for 15 min at 4°C, and stored at −80°C until use. Recombinant MAP2c was expressed and purified as described in Gamblin *et al*. (1996).

Preparation of brain lysates and coimmunoprecipitation

C57BL/10 mice were anesthetized with isofluran and killed by decapitation. On dissection, brain tissue (0.5 g) was snap-frozen in liquid nitrogen and ground in a mortar. The brain was homogenized

in 3 ml of 50 mM HEPES/HCl (pH 7.0), 5 mM $MgCl_2$, 1 mM EGTA, 100 mM NaCl, 0.5% Triton X-100, 0.1 mM DTT, 0.5 mg/ml DNase I (Roche), 0.2 mg/ml RNase A (Serva, Heidelberg, Germany), 1 mM phenylmethylsulfonyl fluoride (PMSF), phosphatase inhibitor cocktail 1 (Sigma-Aldrich), phosphatase inhibitor cocktail 2 (Sigma-Aldrich), and CMPI (lysis solution) on ice, using a Dounce homogenizer (20 strokes, one stroke every 30 s). Brain lysates were centrifuged (90,000 × *g* for 60 min), and the supernatant was precleared by rotating it for 2 h at 4°C with protein G agarose beads (Pierce, Rockford, IL). Protein concentrations in supernatant fractions were measured using the BCA Protein Assay Kit (Pierce) and set to 1 mg/ml using lysis solution. Part of the supernatant (lysate) was mixed with an equal volume of 0.4 M Tris/HCl (pH 6.8), 0.5 M DTT, 10% SDS, 50% glycerol, and 0.1% bromophenol blue (SDS-sample buffer) for further analysis. The rest of the lysate was split into 600-µl samples and incubated overnight with either 5 µg anti-P1c, 5 µg mouse IgG, or 10 µg rabbit anti-EGFP (Invitrogen) antibodies. Antibody–antigen complexes were recovered by incubation with 25 µl of protein G agarose beads for 5 h at 4°C, washed four times with lysis buffer, dissolved in SDS-sample buffer, and subjected to IB.

MAP-promoted in vitro assembly of tubulin

For MAP2c-induced MT assembly, samples of recombinant MAP2c in 80 mM PIPES (pH 6.8), 0.5 mM EGTA, and 2 mM $MgCl_2$ (PEM) were mixed with Triton X-100 (final concentration: 0.5%) and incubated for 15 min at 37°C. Aliquots containing 1 µM of protein were then mixed with 5 µM phosphocellulose (PC)-purified tubulin (in PEM supplemented with 1 mM GTP and 1 mM DTT) and incubated for 1 h at 37°C. For assessing the effect of plectin protein fragments p20-21 and p16-21 on MAP2c-induced MT assembly, 1–60 µM of purified p20-21 or 2–16 µM of purified p16-21 proteins (in PEM) were mixed with MAP2c prior to treatment with Triton X-100 and then mixed with 5 µM PC-purified tubulin (in PEM supplemented with 1 mM GTP and 1 mM DTT). The MTs formed were sedimented by centrifugation. The resulting soluble and pellet fractions each were divided in half, and duplicate samples were analyzed by SDS-10% PAGE (MAP2c and tubulin) and SDS-15% PAGE (p20-21). The formation of intact MTs was routinely monitored by EM of uranyl acetate–stained specimens.

Endogenous Tau–MT binding assay

The protocol of this assay was based on a similar one described by Planel *et al*. (2008); except where indicated otherwise, all working steps were carried out above 20°C to prevent MT depolymerization. Brains isolated from mice were homogenized in 80 mM MES (pH 6.8), 1 mM $MgCl_2$, 2 mM EGTA, 30% glycerol, 0.1% Triton X-100, 1 mM PMSF, 1 mM Na_3VO_4, 1 mM NaF, and CMPI using a mechanical tissue homogenizer. Lysates were centrifuged for 6 min at 16,000 × *g* to obtain supernatant fraction containing intact MTs. Mixtures of the MT fraction and p20-21 (0–70 µM) were incubated for 15 min at 37°C and then centrifuged (20 min at 25°C) in a vacuum Optima TLX Ultracentrifuge (Beckman) at 40,000 rpm to obtain an MT-free supernatant and an MT-containing pellet fraction. MTs in the pellet fraction were resuspended in 100 mM MES (pH 6.5), 0.5 mM $MgSO_4$, 30% glycerol, 1 mM EGTA, 0.1% Triton X-100, 1 mM Na_3VO_4, 1 mM NaF, 2 mM DTT, 1 mM PMSF, and CMPI. Samples of both fractions were mixed with O+ buffer (O'Farrel, 1975) supplemented with CMPI and boiled 5 min prior to IB.

RT-PCR

Total RNA was extracted from tissues and cells using TriFast reagent (Peqlab, Erlangen, Germany). Aliquots (1 µg) were reverse-transcribed using random hexamer primers and SuperScript II polymerase (Invitrogen). RT-PCR was performed using primers binding to nucleotide sequences in exons 9 and 11 of the mouse tau (*Mtapt*) gene and in exons 5 and 6 of the mouse MAP2 (*Mtap2*) gene. Primer pairs (Supplemental Table S1) were designed using Primer3 (http://frodo.wi.mit.edu/primer3). PCR products were resolved on 1.8% agarose gels and visualized by ethidium bromide staining.

SDS–PAGE and IB

Proteins were separated using standard SDS-6% PAGE or SDS-10% PAGE. For IB, proteins were transferred to nitrocellulose membranes, which were blocked with 5% milk powder in PBS supplemented with 0.5% Tween-20 and incubated with primary, followed by HRP-conjugated secondary, antibodies. Quantification of protein bands was performed using QuantiScan version 1.5 software (Biosoft, Cambridge, UK).

Statistical evaluation

Unless otherwise indicated, comparisons between values of two groups were made using Student's *t* test ($\alpha = 0.05$), and comparisons among values of multiple groups were performed using one-way analysis of variance ($\alpha = 0.05$). The significance between values of individual groups and wild-type values was subsequently determined using the Tukey posthoc test ($\alpha = 0.05$). All statistical analyses were performed using SPSS Statistics version 19 (IBM, Armonk, NY).

ACKNOWLEDGMENTS

We thank A. Akhmanova for donating GFP-EB1 and A. Matus for pET3d/MAP2c. EGFP-tubulin and EGFP-paxillin were kindly provided by J. Wehland (deceased August 16, 2010). We thank K. Gross for excellent technical assistance and M. Castañón for critically reading the manuscript. R.G.V. was supported by DOC-FORTE of the Austrian Academy of Science. L.J. and J.N. were supported by grant CZ.1.05/1.1.00/02.0068 from the European Regional Developmental Fund, and L.J., J.N., and G. Wa. were supported by grant 62p1 from the AKTION Austria–Czech Republic program of the Austrian Agency for International Mobility. This work was supported by grant P23729-B11 from the Austrian Science Research Fund.

REFERENCES

Abrahamsberg C, Fuchs P, Osmanagic-Myers S, Fischer I, Propst F, Elbe-Bürger A, Wiche G (2005). Targeted ablation of plectin isoform 1 uncovers role of cytolinker proteins in leukocyte recruitment. Proc Natl Acad Sci USA 102, 18449–18454.

Ackerl R, Walko G, Fuchs P, Fischer I, Schmuth M, Wiche G (2007). Conditional targeting of plectin in prenatal and adult mouse stratified epithelia causes keratinocyte fragility and lesional epidermal barrier defects. J Cell Sci 120, 2435–2443.

Akhmanova A, Steinmetz MO (2008). Tracking the ends: a dynamic protein network controls the fate of microtubule tips. Nat Rev Mol Cell Biol 9, 309–322.

Andrä K, Kornacker I, Jörgl A, Zörer M, Spazierer D, Fuchs P, Fischer I, Wiche G (2003). Plectin-isoform-specific rescue of hemidesmosomal defects in plectin (–/–) keratinocytes. J Invest Dermatol 120, 189–197.

Andrä K, Lassmann H, Bittner R, Shorny S, Fässler R, Propst F, Wiche G (1997). Targeted inactivation of plectin reveals essential function in maintaining the integrity of skin, muscle, and heart cytoarchitecture. Genes Dev 11, 3143–3156.

Andrä K, Nikolic B, Stöcher M, Drenckhahn D, Wiche G (1998). Not just scaffolding: plectin regulates actin dynamics in cultured cells. Genes Dev 12, 3442–3451.

Andreadis A (2005). Tau gene alternative splicing: expression patterns, regulation and modulation of function in normal brain and neurodegenerative diseases. Biochim Biophys Acta 1739, 91–103.
Bowen JR, Hwang D, Bai X, Roy D, Spiliotis ET (2011). Septin GTPases spatially guide microtubule organization and plus end dynamics in polarizing epithelia. J Cell Biol 194, 187–197.
Bulinski JC, Richards JE, Piperno G (1988). Posttranslational modifications of α tubulin: detyrosination and acetylation differentiate populations of interphase microtubules in cultured cells. J Cell Biol 106, 1213–1220.
Burgstaller G, Gregor M, Winter L, Wiche G (2010). Keeping the vimentin network under control: cell-matrix adhesion-associated plectin 1f affects cell shape and polarity of fibroblasts. Mol Biol Cell 21, 3362–3375.
Conde C, Cáceres A (2009). Microtubule assembly, organization and dynamics in axon and dendrites. Nat Rev Neurosci 10, 319–332.
Dehmelt L, Halpain S (2005). The MAP2/Tau family of microtubule-associated proteins. Genome Biol 6, 204.
Dephoure N, Zhou C, Villén J, Beausoleil SA, Bakalarski CE, Elledge SJ, Gygi SP (2008). A quantitative atlas of mitotic phosphorylation. Proc Natl Acad Sci USA 105, 10762–10767.
Duff K *et al*. (2000). Characterization of pathology in transgenic mice overexpressing human genomic and cDNA tau transgenes. Neurobiol Dis 7, 87–98.
Fletcher LM, Welsh GI, Oatey PB, Tavaré JM (2000). Role for the microtubule cytoskeleton in GLUT4 vesicle trafficking and in the regulation of insulin-stimulated glucose uptake. Biochem J 352, 267–276.
Fuchs P *et al*. (2009). Targeted inactivation of a developmentally regulated neural plectin isoform (Plectin 1c) in mice leads to reduced motor nerve conduction velocity. J Biol Chem 284, 26502–26509.
Fuchs P, Zörer M, Rezniczek GA, Spazierer D, Oehler S, Castañón MJ, Hauptmann R, Wiche G (1999). Unusual 5′ transcript complexity of plectin isoforms: novel tissue-specific exons modulate actin binding activity. Hum Mol Genet 8, 2461–2472.
Gache Y, Chavanas S, Lacour JP, Wiche G, Owaribe K, Meneguzzi G, Ortonne JP (1996). Defective expression of plectin/HD1 in epidermolysis bullosa simplex with muscular dystrophy. J Clinic Invest 97, 2289–2298.
Gache V, Waridel P, Winter C, Juhem A, Schroeder M, Shevchenko A, Popov AV (2010). *Xenopus* meiotic microtubule-associated interactome. PLoS One 5, e9248.
Gamblin TC, Nachmanoff K, Halpain S, Williams RC, Jr. (1996). Recombinant microtubule-associated protein 2c reduces the dynamic instability of individual microtubules. Biochemistry 35, 12576–12586.
Gregor M, Zeöld A, Oehler S, Marobela KA, Fuchs P, Weigel G, Hardie DG, Wiche G (2006). Plectin scaffolds recruit energy-controlling AMP-activated protein kinase (AMPK) in differentiated myofibres. J Cell Sci 119, 1864–1875.
Gu Y, Oyama F, Ihara Y (1996). Tau is widely expressed in rat tissues. J Neurochem 67, 1235–1244.
Herrmann H, Wiche G (1987). Plectin and IFAP-300K are homologous proteins binding to microtubule-associated proteins 1 and 2 and to the 240-kilodalton subunit of spectrin. J Biol Chem 262, 1320–1325.
Karr TL, White HD, Purich DL (1979). Characterization of brain microtubule proteins prepared by selective removal of mitochondrial and synaptosomal components. J Biol Chem 254, 6107–6111.
Kaverina I, Krylyshkina O, Small JV (2002). Regulation of substrate adhesion dynamics during cell motility. Int J Biochem Cell Biol 34, 746–761.
Kaverina I, Straube A (2011). Regulation of cell migration by dynamic microtubules. Semin Cell Dev Biol 22, 968–974.
Kodama A, Karakesisoglou I, Wong E, Vaezi A, Fuchs E (2003). ACF7: an essential integrator of microtubule dynamics. Cell 115, 343–354.
Konieczny P, Fuchs P, Reipert S, Kunz WS, Zeöld A, Fischer I, Paulin D, Schröder R, Wiche G (2008). Myofiber integrity depends on desmin network targeting to Z-disks and costameres via distinct plectin isoforms. J Cell Biol 181, 667–681.
Kostan J, Gregor M, Walko G, Wiche G (2009). Plectin isoform-dependent regulation of keratin-integrin α6β4 anchorage via Ca^{2+}/calmodulin. J Biol Chem 284, 18525–18536.
Krylyshkina O, Kaverina I, Kranewitter K, Steffen W, Alonso MC, Cross RA, Small JV (2002). Modulation of substrate adhesion dynamics via microtubule targeting requires kinesin-1. J Cell Biol 156, 349–359.
Lechler T, Fuchs E (2007). Desmoplakin: an unexpected regulator of microtubule organization in the epidermis. J Cell Biol 176, 147–154.
Lee G (2005). Tau and src family tyrosine kinases. Biochim Biophys Acta 1739, 323–330.
Lee G, Newman ST, Gard DL, Band H, Panchamoorthy G (1998). Tau interacts with src-family non-receptor tyrosine kinases. J Cell Sci 111, 3167–3177.
Lim RW, Halpain S (2000). Regulated association of microtubule-associated protein 2 (MAP2) with Src and Grb2: evidence for MAP2 as a scaffolding protein. J Biol Chem 275, 20578–20587.
Liu SY, Chen YT, Tseng MY, Hung CC, Chiang WF, Chen HR, Shieh TY, Chen CH, Jou YS, Chen JY (2007). Involvement of microtubule-associated protein 2 (MAP2) in oral cancer cell motility: a novel biological function of MAP2 in non-neuronal cells. Biochem Biophys Res Commun 366, 520–525.
Ludin B, Ashbridge K, Fünfschilling U, Matus A (1996). Functional analysis of the MAP2 repeat domain. J Cell Sci 109, 91–99.
Mack GJ, Compton DA (2001). Analysis of mitotic microtubule-associated proteins using mass spectrometry identifies astrin, a spindle associated protein. Proc Natl Acad Sci USA 98, 14434–14439.
Malik R, Lenobel R, Santamaria A, Ries A, Nigg EA, Körner R (2009). Quantitative analysis of the human spindle phosphoproteome at distinct mitotic stages. J Proteome Res 8, 4553–4563.
Nikolic B, Mac Nulty E, Mir B, Wiche G (1996). Basic amino acid residue cluster within nuclear targeting sequence motif is essential for cytoplasmic plectin-vimentin network junctions. J Cell Biol 134, 1455–1467.
O'Farrel PH (1975). High resolution two-dimensional electrophoresis of proteins. J Biol Chem 250, 4007–4021.
Ortega E, Buey RM, Sonnenberg A, de Pereda JM (2011). The structure of the plakin domain of plectin reveals a non-canonical SH3 domain interacting with its fourth spectrin repeat. J Biol Chem 286, 12429–12438.
Osmanagic-Myers S, Gregor M, Walko G, Burgstaller G, Reipert S, Wiche G (2006). Plectin-controlled keratin cytoarchitecture affects MAP kinases involved in cellular stress response and migration. J Cell Biol 174, 557–568.
Osmanagic-Myers S, Wiche G (2004). Plectin-RACK1 (receptor for activated C kinase 1) scaffolding: a novel mechanism to regulate protein kinase C activity. J Biol Chem 279, 18701–18710.
Piperno G, LeDizet M, Chang XJ (1987). Microtubules containing acetylated α-tubulin in mammalian cells in culture. J Cell Biol 104, 289–302.
Planel E *et al*. (2008). Anesthesia-induced hyperphosphorylation detaches 3-repeat tau from microtubules without affecting their stability in vivo. J Neurosci 28, 12798–12807.
Pooler AM, Usardi A, Evans CJ, Philpott KL, Noble W, Hanger DP (2012). Dynamic association of tau with neuronal membranes is regulated by phosphorylation. Neurobiol Aging 33, e27–e38.
Poorkaj P, Kas A, D'Souza I, Zhou Y, Pham Q, Stone M, Olson MV, Schellenberg GD (2001). A genomic sequence analysis of the mouse and human microtubule-associated protein tau. Mamm Genome 12, 700–712.
Rezniczek GA, Abrahamsberg C, Fuchs P, Spazierer D, Wiche G (2003). Plectin 5′-transcript diversity: short alternative sequences determine stability of gene products, initiation of translation and subcellular localization of isoforms. Hum Mol Genet 12, 3181–3194.
Rezniczek GA, de Pereda JM, Reipert S, Wiche G (1998). Linking integrin α6β4-based cell adhesion to the intermediate filament cytoskeleton: direct interaction between the β4 subunit and plectin at multiple molecular sites. J Cell Biol 141, 209–225.
Rezniczek GA, Janda L, Wiche G (2004). Plectin. Methods Cell Biol 78, 721–755.
Rogov VV, Rozenknop A, Rogova NY, Löhr F, Tikole S, Jaravine V, Güntert P, Dikic I, Dötsch V (2012). A universal expression tag for structural and functional studies of proteins. Chembiochem 13, 959–963.
Rottner K, Krause M, Gimona M, Small JV, Wehland J (2001). Zyxin is not colocalized with vasodilator-stimulated phosphoprotein (VASP) at lamellipodial tips and exhibits different dynamics to vinculin, paxillin, and VASP in focal adhesions. Mol Biol Cell 12, 3103–3113.
Rouzier R *et al*. (2005). Microtubule-associated protein tau: a marker of paclitaxel sensitivity in breast cancer. Proc Natl Acad Sci USA 102, 8315–8320.
Sauer G, Körner R, Hanisch A, Ries A, Nigg E, Silljé HH (2005). Proteome analysis of the human mitotic spindle. Mol Cell Proteomics 4, 35–43.
Shelanski ML, Gaskin F, Cantor CR (1973). Microtubule assembly in the absence of added nucleotides. Proc Natl Acad Sci USA 70, 765–768.
Smith FJ *et al*. (1996). Plectin deficiency results in muscular dystrophy with epidermolysis bullosa. Nat Genet 13, 450–457.
Spurny R, Gregor M, Castañón MJ, Wiche G (2008). Plectin deficiency affects precursor formation and dynamics of vimentin networks. Exp Cell Res 15, 3570–3580.
Stepanova T, Slemmer J, Hoogenraad CC, Lansbergen G, Dortland B, De Zeeuw CI, Grosveld F, van Cappellen G, Akhmanova A, Galjart N (2003). Visualization of microtubule growth in cultured neurons via the use of EB3-GFP (end-binding protein 3-green fluorescent protein). J Neurosci 23, 2655–2664.

Su LK, Burrell M, Hill DE, Gyuris J, Brent R, Wiltshire R, Trent J, Vogelstein B, Kinzler KW (1995). APC binds to the novel protein EB1. Cancer Res 55, 2972–2977.
Svitkina TM, Verkhovsky AB, Borisy GG (1996). Plectin sidearms mediate interaction of intermediate filaments with microtubules and other components of the cytoskeleton. J Cell Biol 135, 991–1007.
Usardi A, Pooler AM, Seereeram A, Reynolds CH, Derkinderen P, Anderton B, Hanger DP, Noble W, Williamson R (2011). Tyrosine phosphorylation of tau regulates its interactions with Fyn SH2 domains, but not SH3 domains, altering the cellular localization of tau. FEBS J 278, 2927–2937.
Vallee RB (1986). Reversible assembly purification of microtubules without assembly-promoting agents and further purification of tubulin, microtubule-associated proteins, and MAP fragments. Methods Enzymol 134, 89–104.
Vanier MT, Neuville P, Michalik L, Launay JF (1998). Expression of specific tau exons in normal and tumoral pancreatic acinar cells. J Cell Sci 111, 1419–1432.
Walko G *et al*. (2011). Targeted proteolysis of plectin isoform 1a accounts for hemidesmosome dysfunction in mice mimicking the dominant skin blistering disease EBS-Ogna. PLoS Genet 7, e1002396.
Watanabe T, Noritake J, Kaibuchi K (2005). Regulation of microtubules in cell migration. Trends Cell Biol 15, 76–83.
Wiche G (1998). Role of plectin in cytoskeleton organization and dynamics. J Cell Sci 111, 2477–2486.
Wiche G, Briones E, Hirt H, Krepler R, Artlieb U, Denk H (1983). Differential distribution of microtubule-associated proteins MAP-1 and MAP-2 in neurons of rat brain and association of MAP-1 with microtubules of neuroblastoma cells (clone N2A). EMBO J 2, 1915–1920.
Wiche G, Briones E, Koszka C, Artlieb U, Krepler R (1984). Widespread occurrence of polypeptides related to neurotubule-associated proteins (MAP-1 and MAP-2) in non-neuronal cells and tissues. EMBO J 3, 991–998.
Wiche G, Winter L (2011). Plectin isoforms as organizers of intermediate filament cytoarchitecture. BioArchitecture 1, 14–20.
Winter L, Abrahamsberg C, Wiche G (2008). Plectin isoform 1b mediates mitochondrion-intermediate filament network linkage and controls organelle shape. J Cell Biol 181, 903–911.
Winter L, Wiche G (2013). The many faces of plectin and plectinopathies: pathology and mechanisms. Acta Neuropathol 125, 77–93.
Wu X, Kodama A, Fuchs E (2008). ACF7 regulates cytoskeletal-focal adhesion dynamics and migration and has ATPase activity. Cell 135, 137–148.
Yamada K, Nakata M, Horimoto N, Saito M, Matsuoka H, Inagaki N (2000). Measurement of glucose uptake and intracellular calcium concentration in single, living pancreatic ß-cells. J Biol Chem 275, 22278–22283.
Yang Y, Bauer C, Strasser G, Wollman R, Julien JP, Fuchs E (1999). Integrators of the cytoskeleton that stabilize microtubules. Cell 98, 229–238.
Zaid H, Antonescu CN, Randhawa VK, Klip A (2008). Insulin action on glucose transporters through molecular switches, tracks and tethers. Biochem J 413, 201–215.